Università degli Studi del Piemonte Orientale
"Amedeo Avogadro"

Dipartimento di Scienze e Innovazione Tecnologica

Laurea magistrale in Scienze Chimiche

Anno Accademico 2023/2024

Accurate quantum mechanical description of environment effects on Singlet-Triplet Inversion: role of state specific polarization response and dispersion interactions

Relatore:
Prof. Ciro A. Guido

Candidata:
Ester Salvi
mat. 20036924

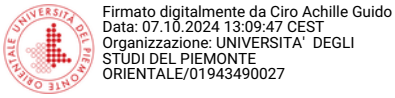

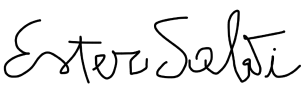

Contents

Chapter 1

Introduction

Materials that interact with light, either absorbing, emitting it or both, form a central part of our daily lives and find applications in a vast range of technologies, from photovoltaics to displays. Therefore, it is becoming increasingly crucial to enhance the functional properties of such materials by developing a detailed understanding of the underlying mechanism: this entails a thorough understanding of molecular excited states.

The electronic structure of a molecule is determined by the quantum behavior of electrons inside the system, resulting in molecular states with different symmetries and different spin multiplicities.

Moreover, another factor that has to be taken into account is the effect of the environment in which the molecule is immersed, which can greatly alter its states and the corresponding spectroscopic signals (positions, intensity and shapes of the bands). A solvent behaves both as a macroscopic continuum characterized only by physical constants (dielectric constant, index of refraction, etc) and a discontinuum medium which consists of individual, mutually interacting solvent molecules.

The interactions between species in solvents (and in solutions) are too strong to be treated by the laws of the kinetic theory of gases, yet too weak to be treated by the laws of solid-state physics. The changes in excited states induced by the environment are a result of such forces, that can be divided into two categories: the first category comprises the so-called directional, induced and dispersion forces, which are non-specific and cannot be completely saturated; the second group consists of specific interactions, such as hydrogen-bonding forces, or electron-pair donor acceptor forces. The main interactions are electrostatic in origin, such as the polarity and the local organization of solvent molecules around the solute molecule. This behavior gives rise to a large use of averaged pictures to model the solute-solvent interactions, such as continuum models. However, to accurately describe the changes in the spectroscopic behavior induced by the medium, a discrete description also for

solvent molecules is needed, to include effects that arise from alteration of the chemical nature of the solvated molecules by the medium (eg.proton or electron transfer, ionization, etc) or specific interactions, such as hydrogen bonding.

From the above discussion, it is clear that the understanding of excited state properties requires and adequate combination of electronic structure method and solvation model. The aim of the work presented in this thesis is to provide an accurate description of the effects of solvation on Inverted Singlet-Triplet (IST) organic emitters. These substrates have attracted growing interest as potential candidates for Organic Light Emitting Diodes (OLEDs) with improved efficiency with respect to Thermally Activated Delayed Fluorescence (TADF) molecules. IST substrates with significant fluorescence rates could surpass TADF-based emitters by facilitating a rapid, non-activated reverse intersystem crossing process (rISC).[1] Electron correlation has been proved to be crucial in predicting a negative ΔE_{ST}[2, 3], given the doubly-excited character of the charge-transfer excited states involved. Ehrmaier et al. were the first to demonstrate singlet-triplet inversion in heptazine using wavefunction methods,[4] whereas De Silva independently confirmed this phenomenon in cyclazine.[3]. Subsequently, further evidence was obtained both computationally and experimentally for larger substituted heptazines[5–7]. A variety of modeling approaches with different computational costs have been tested so far on IST candidates, ranging from double-hybrid TD-DFT[8] and CIS(D)[9] to coupled-cluster methods[8, 10, 11], as well as multireference[9, 10] and multiconfigurational[4, 8–10] techniques. In a study by Jacquemin et al.[11], predictions of vertical singlet-triplet inversion energies *in vacuo* for a set of 10 triangulene cores were made using coupled-cluster (CC) methods with large basis sets providing theoretical best estimates of ΔE_{ST}s. Additionally, the impact of geometrical relaxation and vibrational corrections on singlet-triplet gaps was analyzed and rationalized, leading to the conclusion that accounting for adiabatic effects does not significantly alter the vertical approximation of the singlet-triplet gap. More recently, using the PPP hamiltonian approach, Bedogni et al. have reassessed the significance of molecular symmetry and connectivity in relation to ST gap inversion in favour of the importance of spin-polarization arising from a small HOMO-LUMO exchange energy.[12] However, to the best of our knowledge, a comprehensive study of the effects of solvation on molecules exhibiting singlet-triplet inversion has not yet been conducted. In the simulation of environmental effects on the formation and relaxation of electronic excited states, it is crucial to include non-equilibrium effects as well as a diverse description of the embedding's polarization response.[13] Previous studies on singlet excited states have highlighted the significance of incorporating state-specific corrections into conventional LR-PCM to recover the contribution of the response of the solvent due to the density reorganisation.[14] Moreover, a rigorous derivation of

the PCM equations for a quantum solute in an electrostatic environment, based on the theory of open quantum systems, has demonstrated that the solvated excited-state energies must incorporate a dispersion term.[15] Depending on the expression used for dispersion, the LR-PCM energy can recover part of the solute-solvent dispersion interaction.[16, 17] On the other hand, recovering solvent-solute dispersion proves more complex. Marenich et al. proposed a potential approach that involves treating the dispersion contribution as a semiempirical correction derived from the solute polarizability.[18] However, the model in question was parameterized solely for singlet excited states and could not be be readily extended to triplets, which are crucial for the scope of our study. In this paper, we present a computational protocol for determining the first singlet and triplet excited-state energies of solvated IST systems, with the objective of capturing the various contributions resulting from interactions with the environment. The accurate description of solvent effects must be coupled with a correspondingly reliable electronic structure model. With this in mind, will provide a definition for the S_1 and T_1 adiabatic energies, herein referred to as $E(ExS)_{\mathbf{ss\text{-}pol+disp}}$, that contains a second-order perturbative correction, derived from double-hybrid TD-DFT/B2PLYP calculations, applied to the SS excitation energies. The method was initially benchmarked on heptazine and cyclazine and subsequently extended to systems of experimental relevance. The text is organised as follows:

- Chapter 2 presents an overview on Thermally Activated Delayed Fluorescence and Singlet-Triplet Inversion, as well as a brief description of their application in OLEDs

- Chapter 3 includes the theoretical background: DFT and TD-DFT are shortly described, with a focus on the functionals used over the course of the study; the PCM framework and excited state solvation models are then described;

- Chapter 4 contains the details of the computational study that leads to the formulation of a new computational protocol for modelling IST system interacting with solvents;

- Conclusion remarks and new perspectives are given in chapter 5.

Chapter 2

TADF and INVEST emitters

2.1 Organic Light Emitting Diodes

Materials that emit light have undergone a significant evolution in the last 20 to 30 years, with light emitting diodes (LEDs) gradually passing by plasma and liquid crystal displays. More recently, LEDs have found a competitor in Organic Light Emitting Diodes (OLEDs). The latter involve organic materials, which are easier to handle and manufacture, and might be valuable candidates for transparent and/or flexible displays.[19, 20]

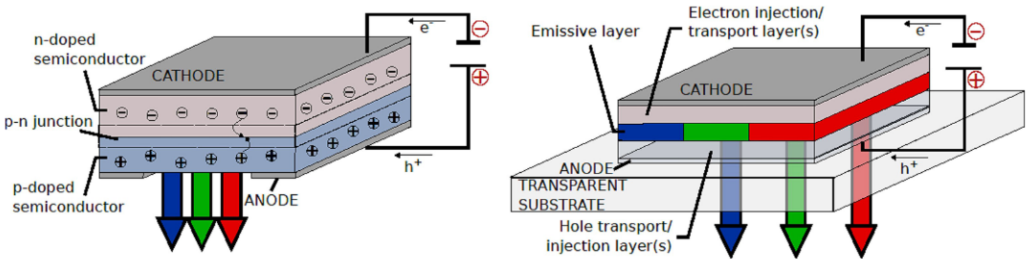

Figure 2.1: Representation of the architecture for LEDs (left) and OLEDs (right) (Eng and Penfold, 2020)

Figure 2.1 shows the key differences between the two diodes. The core of a traditional LED is the **p-n junction**, which is the boundary between two semiconductor materials: the p-type and the n-type. In a p-type (positive) semiconductor there is an excess of positively charged carriers ('holes') while in a n-type (negative) material there are more electrons. When these two materials are joined, a depletion region forms at the interface, where electrons from the n-type material recombine with holes from the p-type material. This creates an electric field that allows the

p-n junction to act as a diode, conducting current in one direction but blocking it in the opposite direction.[21]
On the other hand, an OLED is made of several layers of organic materials, stacked between two electrodes. If a current is applied to the electrodes, electrons and holes migrate towards the emissive layer, where they recombine to form emissive spin-singlet states, as well as non-emissive triplet states.
In contrast to the selection rules associated with photo-excitation, this process of exciton generation leads to a 1:3 singlet to triplet population. Thus, when adopting a typical organic molecule, as in the case of first generation fluorescent OLEDs, only 25% of the generated excited states are harvested.
A second generation of OLEDs, often referred to as phosphorescence OLEDs, known as PhOLEDs, have been developed, in order to overcome the loss of the remaining 75% of excitons. These devices contain heavy elements to promote spin-orbit coupling and, therefore, activate phosphorescence. This mechanism results in the harvest of 100% of excited states. However, only third row transition metals have, to date, exhibited phosphorescence lifetimes short enough for applications in OLEDs. Complexes of such metals are also toxic, expensive and often unstable. These strong disadvantages make them unsuitable for most applications, despite their high efficiency.
Recently, the need to get round the use of heavy metals has led to a significant amount of research on the third generation of OLEDs, that exploit the thermally activated delayed fluorescence (TADF) mechanism.[22] In all cases, a key role in determining the efficiency of OLEDs is played by the lifetime of the triplet excited states and the communication between the singlet and triplet manifold. Therefore, a combination of radiative and non-radiative decay processes, such as luminescence, internal conversion (IC), intersystem crossing (ISC) and electron/energy transfer, need to be understood in detail in order to enhance excited state design of functional materials. This is where the theoretical and computational approach to the problem becomes crucial.

2.2 Thermally Activated Delayed Fluorescence

Prompt fluorescence is a two-step process, which involves the generation of an electronically excited state followed by its subsequent radiative decay into the electronic ground state. However, a more complicated route, involving the triplet manifold, is also available for fluorescence to occur. In this instance, given that spin-orbit coupling is not null, the singlet excited state decays into the triplet state via intersystem

crossing (ISC). Then, provided that both the phosphorescence and non-radiative decay are sufficiently slow and the energy gap between the singlet and triplet excited state is small enough, a reverse intersystem crossing (rISC) back to the singlet state can occur. rISC is subsequently followed by emission and, therefore, the mechanism is known as delayed fluorescence (DF). Since the pioneering work of Adachi and co-workers[20], who exploited the rISC of DF to harvest the triplet states of molecules generated under electric excitation within an organic light emitting diodes and demonstrated high efficiency electroluminescence for the first time using only organic molecules, the mechanism is widely referred to as Thermally Activated Delayed Fluorescence (TADF).

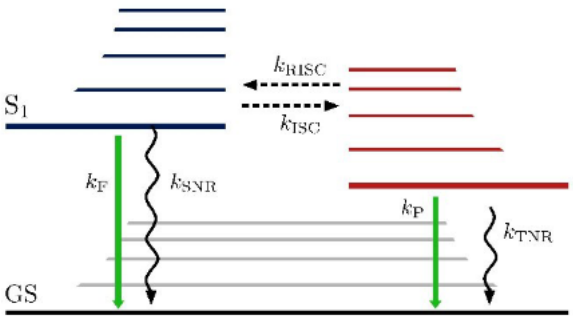

Figure 2.2: A schematic Jablonski diagram accounting for all the radiative and non-radiative processes that involve the first singlet and triplet excited states (Eng and Penfold 2020)

TADF emitters present apparently contradictory requirements. Indeed, the molecules should have a large radiative rate, but also a small gap between the lowest singlet and triplet states. In fact, a small gap between the lowest-lying singlet and triplet state (Δ E_{ST}= E_{S_1} -E_{T_1}) enables a thermal up-conversion from the triplet to the singlet manifold and subsequent fluorescence from the bright S_1 state. Therefore, when designing TADF emitters, one has to make sure that the molecules have donor and acceptor units with spatially separated highest occupied molecular orbital (HOMO) and lowest unoccupied molecular orbital (LUMO), which give rise to excited states with predominantly charge-transfer (CT) character. A CT state is characterised by small exchange couplings that allow for a significant equilibrium population in the S_1 state.
However, a pure CT character would inhibit efficient rISC and fluorescence, implying that a low-lying local excitation (LE) also plays a role in the TADF mechanism.

The strategies for developing efficient TADF emitters thus need to include a thorough understanding of the mixed LE/CT nature of the excited states, as well as the importance of vibronic effects and the influence of the interactions with the environment.[23]

2.3 Singlet-Triplet Inversion

Exchange interactions are responsible for stabilizing triplets and destabilizing singlets, leading to a positive (Δ E_{ST}= E_{S_1} -E_{T_1}) for the vast majority of molecular systems. However, if one were to design a molecule with an inverted singlet-triplet gap, the up-conversion in TADF would be replaced by a more efficient down-conversion. When it comes to predicting if a molecule could possess such property, there is still no indisputable ab initio prediction of a molecular system with inverted singlet and triplet states and gaining such information would allow for a rational design of OLED emitters with improved efficiency.
At present, it remains unclear which electronic structure requirements are necessary for a molecule to exhibit such inversion. What has been clarified by De Silva is the crucial role played by electronic correlation in the description of the singlet-triplet inversion, as well as that of the interaction with a polarizable environment.[1, 3]
To support the first conclusion, he showed that a non-correlated method, such as Configuration Interaction Singles (CIS) or Time-Dependent Hartree-Fock (TD-HF), cannot predict inverted gaps. The same can be said for TD-DFT, when a frequency-independent kernel is used (adiabatic approximation), since this method generally fails to describe double excitations. [24] This points to the need to resort to wave-function methods that explicitly include doubles or use TD-DFT with double hybrid functionals, that account for double excitations through a perturbative correction.[25, 26]. Further studies have then demonstrated the possibility of predicting a negative ΔE_{ST} through the choice of an appropriate DFT-based method[27].
Moreover, the presence of a polarizable embedding scheme might effectively mimic the effect of including double excitations in the wave function of the entire system and could therefore induce a negative ST gap.

Chapter 3

Methods

3.1 Time Dependent Density Functional Theory excited states

In general, when performing a calculation of energies and other properties of the electronic excited states, one has to take into account the computational cost of the method as well as its accuracy.
The Kohn-Sham (KS) approach to Density Functional Theory (DFT), which is currently used extensively for the description ground electronic states, usually represents a favorable choice from both points of view. Likewise, the Time-Dependent Density Functional Theory (TD-DFT) could be a valuable candidate for evaluating excited-state geometries and properties. We will shortly discuss both methods in the following paragraphs.
Moreover, a brief explanation of the Møller–Plesset perturbation theory will be provided, in the context of the recently formulated double-hybrid functionals. Such functionals were extensively used for the calculations presented in these thesis.
In the end, given the importance of INVEST emitters interaction with the embedding, we will provide a review of the Polarizable Continumm Model. In particular, we will describe three possible schemes for excited-state solvation.

3.1.1 Short overview of Density Functional Theory

Throughout the presentation of the theory, we will rely on the Born-Oppenheimer approximation in order to separate the nuclear from the electronic part of the Schrödinger equation. Our focus will be on the electronic problem, that in the time-independent non-relativistic formulation is written as follows (in atomic units):

$$\hat{H}^e|\Psi(x_1...x_i...x_N)\rangle = E|\Psi(x_1...x_i...x_N)\rangle \tag{3.1}$$

Here, we have:

$$x = r\sigma \tag{3.2}$$

$$\hat{H}^e = \sum_i^N \hat{t}_i + \sum_i^N \hat{v}_{ext}(r_i) + \frac{1}{2}\sum_{i,j\neq i}^N \frac{1}{|r_i - r_j|} = \hat{T} + \hat{V} + \hat{W} \tag{3.3}$$

$$\hat{t_i} = -\frac{1}{2}\nabla_i^2 \tag{3.4}$$

$$\hat{v}_{ext}(r_i) = \sum_\alpha^{N_{nuc}} \frac{Z_\alpha}{|r_i - R_\alpha|} \tag{3.5}$$

The many-particle wave function $\Psi(x_1...x_i...x_N)$ contains all the information of the system. Now, the energy is an exact functional solely of the first order density matrix, and of the diagonal of the second order density matrix[28]. These are defined as:

$$\Gamma^{(1)}(x_1^{'}|x_1) = N\int dx_2...dx_N \Psi(x_1^{'}...x_i^{'}...x_N^{'})\Psi(x_1...x_i...x_N) \tag{3.6}$$

$$\Gamma^{(2)}(x_1^{'}, x_2^{'}|x_1, x_2) = \binom{N}{2}\int dx_3...dx_N \Psi(x_1^{'}...x_i^{'}...x_N^{'}) \tag{3.7}$$

We can therefore write:

$$E = \int dx[\frac{1}{2}\nabla^2\Gamma^{(1)}(x|x^{'})]_{x=x^{'}} + \int dx v_{ext}(\vec{x})\gamma^{(1)}(x) + \int dx \int dx^{'}\frac{1}{|\vec{r} - \vec{r'}|}\gamma^{(2)}(x, x^{'}) \tag{3.8}$$

$$\gamma^{(1)} = \Gamma^{(1)}(x|x) \tag{3.9}$$

$$\gamma^{(2)}(x, x^{'}) = \Gamma^{(2)}(x, x^{'}|x, x^{'}) \tag{3.10}$$

The electron density and the energy are then defined as:

$$\rho(r) = \sum_\sigma \gamma^{(1)}(r\sigma) \tag{3.11}$$

$$E = E[\Gamma^{(2)}] \tag{3.12}$$

In principle, we would be able to obtain the wave function and density of the system by solving the Schrödinger equation and could thus write: $\hat{v}_{ext} \rightarrow \rho(r)$.[29] This is the starting point for both the first and second Hohenberg-Kohn theorem.[30]

Theorem 1 (of Hohenberg and Kohn) *The external potential is (to within an additive constant) a unique functional of the ground state density and therefore:*

$$v_{ext}(r) \leftrightarrow \rho(r) \tag{3.13}$$

Corollarium 1 *The ground state expectation value of any observable $\hat{O}$ is a unique functional of the exact ground state density*:

$$O[\rho] = \langle \Psi[\rho] | \hat{O} | \Psi[\rho] \rangle \tag{3.14}$$

Therefore:

$$E[\rho] = T[\rho] + W[\rho] + V[\rho] = F_{HK}[\rho] + V[\rho] \tag{3.15}$$

$F_{HK}[\rho]$ is generally referred to as *universal* functional, because it does not depend on the external potential.

Theorem 2 (variational character of Energy Functional) *Given the exact ground state density ρ_0 for an external potential v_0, and a different v-representable density ρ,*

$$E_{v0}[\rho_0] \leq E_{v0}[\rho] \tag{3.16}$$

Now problems arise mainly, but not only, because the form of exact universal functional is unknown. The Kohn-Sham scheme represents a valid strategy to overcome this issue and relies on using a model system of non-interacting electrons. This is the central assertion of the Kohn-Sham scheme:
For each interacting system, there must be a local monoelectronic potential v_s , such that the exact density of the interacting system is equal to the density of the non-interacting system with external potential v_s. In the K-S formulation, the density is expressed in terms of N orthonormal orbitals,

$$\rho(r) = \sum_i = |\phi_i(r)|^2 \tag{3.17}$$

and the universal functional is:

$$F_{KS}[\rho] = -\frac{1}{2} \sum_i \langle \phi_i | \nabla^2 | \phi_i \rangle + E_H[\rho] + E_{XC}[\rho] \tag{3.18}$$

E_H represents the Hartree (or Coulomb) energy and is given by:

$$E_H[\rho] = \frac{1}{2} \int \int \frac{\rho(r_1)\rho(r_2)}{r_{12}} dr_1 dr_2 \tag{3.19}$$

E_{XC}, on the other hand, is the exchange-correlation (XC) energy functionals, which accounts for electron-electron interaction and the correction to the kinetic energy of the interacting system. Minimizing the energy of the system gives the Kohn-Sham equation:

$$\hat{f}_i^s[\rho]\phi_i(r) = \epsilon_i \phi_i(r) \tag{3.20}$$

Here, we defined a single-particle Kohn-Sham hamiltonian[31]:

$$\hat{f}_i^s = -\frac{1}{2}\nabla^2 + v_s(r) + v_H[\rho](r) + v_{XC}[\rho](r) \tag{3.21}$$

a Hartree potential:

$$v_H[\rho](r) = \frac{\delta E_H(r)}{\delta \rho(r_1)} \tag{3.22}$$

The unknown term is the XC functional, for which an approximation of some kind has to be found. The difference between various DFT methods consists in the choice of approximation. For the purpose of this thesis, a brief review of the Local Density Approximation (LDA), the Generalized Gradient Approximation (GGA), the global hybrid (GH) functionals, as well as of some double hybrid functionals, will be given.
LDA The Local Density Approximation is based on the assumption that the E_{XC} functional of a system whose electron density is not constant ($\rho \neq 0$) can be defined from the same results one gets for a homogeneous electron gas (HEG) :

$$E_{XC}^{LDA}[\rho] = \int \rho(r)\epsilon_{xc}[\rho]dr \tag{3.23}$$

where the exchange-correlation energy density ϵ_{xc} is a function of the density alone. Of course, this expression entails errors of some sort for systems that differ from HEG. For instance, it tends to underestimate by 10 % the exchange energy of the atoms and exhibits a wrong asymptotic behavior.[32]
GGA A large number of methods, developed as alternatives to the local functionals, fall under the name of Generalized Gradient Approximation. The name arises from the quite factual evidence that the density gradient of a common atom or molecule is not zero, as it was in the case of the HEG. In general, a GGA functional is of the type[33]:

$$E_{XC}[\rho, \nabla\rho] = \int \rho(r) f_x(\rho, \nabla\rho, r)dr \tag{3.24}$$

Hybrid functionals Hybrid functionals are linear combinations of the exact exchange functional from Hartree-Fock and any number of explicit exchange and correlation density functionals from other sources (ab initio, such as LDA and GGA, or empirical). The exact exchange energy functional is expressed in terms of the Kohn-Sham orbitals rather than the density, therefore sometimes it is indicated as an implicit density functional. This strategy provides for a more accurate description of different molecular properties, such as bond lenghts and atomization energies.[34]
Double-hybrid functionals The family of *so-called* double-hybrids (DH) has been recently introduced in the context of density functional theory: the first double-hybrid to be formulated is B2PLYP. The motivation behind DH density functionals is similar to that of an hybrid functional. While in the latter only a portion of the

DFT exchange is substituted by Fock-exchange, B2PLYP additionally replaces part of the DFT correlation functional with a nonlocal correlation contribution based on a Møller -Plesset type second-order perturbative treatment (MP2). In a DH-DFT treatment we can write:

$$E_{XC}^{DHDFT} = (1 - a_X)E_X^{DFT} + a_X E_X^{HF} + (1 - a_C)E_C^{DFT} + a_C E_C^{PT2} \tag{3.25}$$

Practically, the B2PLYP energy is obtained in two steps. First, the hybrid part of the functional is solved self-consistently. Subsequently an MP2-type calculation based on the converged KS-orbitals is carried out and the resulting correlation energy is added to the hybrid-DFT result.[25, 35]

3.1.2 Møller-Plesset perturbation theory

In the context of Many Body Perturbation theories, the one proposed by Møller and Plesset has the Hartee-Fock wavefunction as the unperturbed wavefunction and the unperturbed Hamiltionian $\hat{H}^0$ taken as the sum of one-electron Fock operators. The perturbation is then written as[36]

$$\hat{H}' = \hat{H} - \hat{H}^0 = \sum_l \sum_{m>l} \frac{1}{r_{lm}} - \sum_{m=1}^{n} \sum_{j=1}^{n} [\hat{j}_{j(m)} - \hat{k}_{j(m)}] \tag{3.26}$$

where $\hat{j}$ and $\hat{k}$ are the coulomb and exchange operators respectively.
If we denote the ground state with the subscript 0, we then have:

$$E_0^{(0)} + E_0^{(1)} = \langle \Psi_0^0 | \hat{H}^0 | \Psi_0^0 \rangle + \langle \Phi_0 | \hat{H}' | \Phi_0 \rangle = \langle \Phi_0 | \hat{H} | \Phi_0 \rangle \tag{3.27}$$

which is equal to the variational integral for the Hartree-Fock wavefunction and corresponds to the Hartree-Fock energy itself.
Therefore, the second order energy correction (MP2) is the value needed in order to improve on the Hartree-Fock energy:

$$E_0^{(2)} = \sum_{s \neq 0} \frac{|\langle \Psi_s^0 | \hat{H}' | \Phi_0 \rangle|^2}{E_0^{(0)} - E_s^{(0)}} \tag{3.28}$$

3.1.3 The Time Dependent DFT

In order to extend KS-DFT to systems other than ground states, a time-dependent formulation of the two HK theorems and, consequentially, a time-dependent KS equation must be derived.
The theorem Runge-Gross serves exactly this purpose and constitutes the corner-

stone of the time-dependent Kohn-Sham formalism.[37]

Theorem 3 (of Runge and Gross) *The exact time-dependent electron density, $V(r,t)$, determines the time-dependent external potential, $V(r,t)$, up to a spatially constant, time-dependent function $C(t)$ and thus the time-dependent wave function, $\Psi(r,t)$, up to a time dependent phase factor.* The wave function remains a functional of the electron density:

$$\Psi(r,t) = \Psi[\rho(t)](t)e^{-i\alpha t} \tag{3.29}$$

with $(d/dt)\alpha(t) = C(t)$. The definition of $V(t)$ in this case is:

$$V(t) = \sum_{i}^{N} v(r_i, t) \tag{3.30}$$

a time-dependent external potential given as a sum of one-particle potentials.

Linear Response Approach to TD-DFT In order to derive a time-dependent Kohn-Sham equation, one can apply the stationary action principle. The time-dependent Kohn-Sham equation can be expressed in matrix notation in a basis of M time-independent single-particle wave functions $\{\chi_i(r)\}$ such that:

$$\phi_p(r,t) = \sum_{j} c_{pj}\chi_j(r) \tag{3.31}$$

Therefore, the time-dependent KS equation is written as:

$$i\frac{\partial}{\partial t}\mathbf{C} = \mathbf{F}^{KS}\mathbf{C} \tag{3.32}$$

Here, the i-th column of the matrix C contains the time-dependent expansion coefficients of $\phi_i(r,t)$ and FKS is the matrix representation of the time-dependent Kohn-Sham operator in the given basis. If we multiply equation 3.29 from the right for $\mathbf{C}^{\dagger}$ and then subtract its Hermitian transpose from the resultant equation we obtain the Dirac form of the time dependent Kohn-Sham equation in density matrix form:

$$\sum_{q}(F_{pq}P_{qr} - P_{pq}Fqr) = i\frac{\partial}{\partial t}P_{pr} \tag{3.33}$$

Here, the density matrix P_{pr} is related to electron density through this general definition:

$$\rho(r,t) = \sum_{p,r}^{N}\sum_{i,j}^{M} c_{pj}(t)c^{*}_{ri}(t)\chi_j(r)\chi^{*}_i(r) = \sum_{i,j}^{M}\chi_j(r)\chi^{*}_i(r)P_{ij} \tag{3.34}$$

To obtain excitation energies and oscillator strengths employing the time-dependent KS approach, two different strategies can be followed. One possibility is to propagate

the time-dependent KS wave function in time, which is referred to as "real-time TD-DFT". However, the most common approach as well as the one used over the course of this thesis is the one based on the linear response: using a density matrix formalism, it is shown how the excitation energies are obtained from the linear time-dependent response to a time-dependent external electric field of the time-independent ground-state electron density.
Before applying the time-dependent electric field, the system is assumed to be in the electronic ground-state. In the density matrix formulation we can therefore write:

$$\sum_q (F_{pq}^{(0)} P_{qr}^{(0)} - P_{pq}^{(0)} F q r^{(0)}) = 0 \tag{3.35}$$

with the idempotency condition:

$$\sum_q P_{pq}^{(0)} P_{qr}^{(0)} = P_{pr}^{(0)} \tag{3.36}$$

F_{pq}^0 and P_{pq}^0 correspond to the Kohn-Sham Hamiltonian and density matrix of the unperturbed ground state, respectively. The elements of such matrix, in the basis of the orthonormal unperturbed single-particle orbitals of the ground state, are simply given as

$$F_{pq}^{(0)} = \delta_{pq} \epsilon_p \tag{3.37}$$

and

$$\begin{aligned} P_{ij}^{(0)} &= \delta_{ij} \\ P_{ia}^{(0)} = P_{ai}^{(0)} &= P_{ab}^{(0)} \end{aligned} \tag{3.38}$$

We will now analyse the linear response to an oscillatory time-dependent field. In general perturbation theory, we are able to write the density matrix as the sum of the unperturbed ground state and its first-order time-dependent change

$$P_{pq} = P_{pq}^{(0)} + P_{pq}^{(1)} \tag{3.39}$$

as well as the time-dependent Kohn-Sham Hamiltonian, which to first order is given as the sum of the ground-state KS Hamiltonian and the first-order change

$$F_{pq} = F_{pq}^{(0)} + F_{pq}^{(1)} \tag{3.40}$$

Therefore, the time-dependent KS equation, in Dirac form, becomes:

$$\sum_q (F_{pq}^{(0)} P_{qr}^{(1)} - P_{pq}^{(1)} F_{qr}^{(0)} + F_{pq}^{(1} P_{qr}^{(0)} - P_{pq}^{(0)} F_{qr}^{(1)}) = i\frac{\partial}{\partial t} P_{pr}^{(1)} \tag{3.41}$$

The first-order change of the Kohn-Sham Hamiltonian, $F_{pq}^{(1)}$, consists of two terms. The first term corresponds to the applied perturbation, the time dependent electric field itself, and in matrix notation is given as

$$g_{pq} = \frac{1}{2}[f_{pq} e^{-i\omega t} + f_{qp}^* e^{i\omega t}] \tag{3.42}$$

where f_{pq} is a one-electron operator that describes the applied perturbation.
Then, the second term is given as the change in the KS Hamiltonian due to the changes in the density matrix:

$$\Delta F_{pq}^{(0)} = \sum_{st} \frac{\partial F_{pq}^{(0)}}{\partial P_{st}} P_{st}^{(1)} \tag{3.43}$$

such that the first-order change in the KS Hamiltonian is altogether given as:

$$F_{pq}^{(1)} = g_{pq} + \Delta F_{pq}^{(0)} \tag{3.44}$$

The time-dependent change of the density matrix induced by the perturbation of the KS Hamiltonian, this is to first order given as

$$P_{pq}^{(1)} = \frac{1}{2}[X_{pq} e^{-i\omega t} + Y_{qp}^* e^{i\omega t}] \tag{3.45}$$

where X_{pq} and Y_{qp} represent perturbation densities. Now we can rewrite equation 3.40 as:

$$\sum_q [F_{pq}^{(0)} X_{qr} - X_{pq} F_{qr}^{(0)} + (f_{pq} + \sum_{st} \frac{\partial F_{pq}^{(0)}}{\partial P_{st}} X_{st}) P_{qr}^{(0)} - P_{pq}^{(0)} (f_{qr} + \sum_{st} \frac{\partial F_{pq}^{(0)}}{\partial P_{st}} X_{st})] = \omega X_{pr} \tag{3.46}$$

to which we have to add the complex coniugate term, that comes from multiplying the $e^{i\omega t}$ terms. The idempotency condition (Eq.3.36) gives this expression for the first order change of the density matrix of the form

$$\sum_q [P_{pq}^0 P_{qr}^1 + P_{pq}^1 P_{qr}^0] = P_{pq}^0 \tag{3.47}$$

which leads to the following restrictions to the $\mathbf{X}$ matrix:

- occupied-occupied and virtual-virtual blocks (X_{ii},Y_{aa}) are zero

- only the occupied-virtual and virtual-occupied blocks (X_{ia},Y_{ai}) are taken into account.

If we now assume that the electronic transitions occur for an infinitesimal perturbation, which is to say that $f_{ia} = f_{ai} = 0$ (zero-frequency limit), we obtain a non-Hermitian eigenvalue equation, the LR-KS equation:

$$\begin{bmatrix} \mathbf{A} & \mathbf{B} \\ \mathbf{B*} & \mathbf{A*} \end{bmatrix} \begin{bmatrix} \mathbf{X} \\ \mathbf{Y} \end{bmatrix} = \omega \begin{bmatrix} \mathbf{1} & \mathbf{0} \\ \mathbf{0} & \mathbf{-1} \end{bmatrix} \begin{bmatrix} \mathbf{X} \\ \mathbf{Y} \end{bmatrix} \tag{3.48}$$

Where the matrix elements have the following meaning:

$$\begin{aligned} A_{ia\sigma,jb\tau} = \delta_{ij}\delta_{ab}\delta_{\sigma\tau}(\epsilon_a - \epsilon_b) + \langle i_\sigma j_\tau | a_\sigma b_\tau \rangle + \\ -C_{HF}\delta_{\sigma\tau}\langle i_\sigma a_\sigma | j_\tau b_\tau \rangle + \\ +(1 - C_{HF})\langle i_\sigma j_\tau | f_{xc} | a_\sigma b_\tau \rangle \end{aligned} \tag{3.49}$$

$$\begin{aligned} B_{ia\sigma,jb\tau} = \langle i_\sigma b_\tau | a_\sigma j_\tau \rangle - C_{HF}\delta_{\sigma\tau}\langle i_\sigma a_\sigma | j_\tau b_\tau \rangle + \\ +(1 - C_{HF})\langle i_\sigma b_\tau | f_{xc} | a_\sigma j_\tau \rangle \end{aligned} \tag{3.50}$$

The equations above represent the TD-DFT formalism, which is solved to obtain the excitation energies ω and transition vectors. As one can see, the elements of matrices **A** and **B** contain elements both of the XC potential as well as of the Hartree-Fock exchange. Therefore, the equations contain TD-HF and pure TD-DFT as limiting cases: $C_{HF} = 1$ and $C_{HF} = 0$ respectively.

Gradients of LR-KS energies Since a crucial part of this thesis is represented by the calculation of molecular properties of a system in its excited states, we will now briefly describe how the calculation of analytic derivatives of TD-DFT has been implemented in recent years.[38] The derivative of the energy of the excited state K with respect to a generic perturbation ξ

$$E_K^\xi = \frac{\partial E_K}{\partial \xi} \tag{3.51}$$

can be obtained by calculating

$$\omega^\xi = \frac{\partial \omega}{\partial \xi} \tag{3.52}$$

and adding it to

$$E_{GS}^\xi = \frac{\partial E_{GS}}{\partial \xi} \tag{3.53}$$

We now have a derivative expression

$$\omega_K^\xi = \frac{1}{2}\langle \mathbf{X}_K + \mathbf{Y}_K | (\mathbf{A}+\mathbf{B})^\xi | \mathbf{X}_K + \mathbf{Y}_K \rangle + \frac{1}{2}\langle \mathbf{X}_K - \mathbf{Y}_K | (\mathbf{A}-\mathbf{B})^\xi | \mathbf{X}_K - \mathbf{Y}_K \rangle \tag{3.54}$$

that formally requires the knowledge of the change in the elements of Fock matrix in the MO basis which in turn requires the knowledge of the MO coefficients derivatives, which are the solution of the couple perturbed Kohn-Sham equations (CPKS). However, one does not need to solve CPKS equations for each perturbation, but rather only for one degree of freedom, to find the so called Z-vector or relaxed density, which represents the orbital relaxation contribution to the one-particle density matrices involved in all post-SCF gradient expressions.

$$\mathbf{P}^K = \mathbf{P}^0 + \mathbf{P}^K_\Delta \tag{3.55}$$

$$\mathbf{P}^K_\Delta = \mathbf{T}^K + \mathbf{Z}^K \tag{3.56}$$

Here, the $\mathbf{Z}^K$ matrix contains the occupied-virtual blocks of $\mathbf{P}^\Delta$, obtained by solving the so-called Z-vector equation:

$$G^+_{ai\sigma}[P^\Delta_{bj}] + \delta_{ab}\delta_{ij}\delta_{\sigma\sigma'}(\epsilon_{a\sigma} - \epsilon_{i\sigma})P^\Delta_{ai\sigma} = L_{ai\sigma} \tag{3.57}$$

where

$$G^+_{pq\sigma}[P_{rs}] = \sum_{rs\sigma'}[(2pq\sigma|rs\sigma') + 2f^{Xc}_{pq\sigma,rs\sigma'} - c_X\delta_{\sigma\sigma'}[(ps\sigma|rq\sigma') + (pr\sigma|sq\sigma')]]P_{rs\sigma'} \tag{3.58}$$

$$G^-_{pq\sigma}[P_{rs}] = \sum_{rs\sigma'}[[(ps\sigma|rq\sigma') + (pr\sigma|sq\sigma')]]P_{rs\sigma'}] \tag{3.59}$$

and $L_{ai\sigma}$ is the Lagrangian of the system, which depends only from occupied-occupied and virtual-virtual blocks of $\mathbf{P}^\Delta$, i.e. T^K_{ij} and T^K_{ab}

$$L_{ai\sigma} = C_{1ai\sigma} - C_{2ai\sigma} + G^+_{ai\sigma}[P^\Delta_{kl}] + G^+_{ai\sigma}[P^\Delta_{bc}] \tag{3.60}$$

$$\begin{aligned} C_{1ai\sigma} = &\sum_b (X+Y)_{bi\sigma}G^+_{ba\sigma}[(X+Y)_{rs}] \\ &+ \sum_b (X-Y)_{bi\sigma}G^-_{ba\sigma}[(X-Y)_{rs}] \\ &+ \sum_b (X+Y)_{bi\sigma}G^{xc}_{ba\sigma}[(X+Y)_{rs}] \end{aligned} \tag{3.61}$$

$$\begin{aligned} C_{2ai\sigma} = &\sum_j (X+Y)_{aj\sigma}G^+_{ij\sigma}[(X+Y)_{rs}] \\ &+ \sum_j (X-Y)_{aj\sigma}G^-_{ij\sigma}[(X-Y)_{rs}] \end{aligned} \tag{3.62}$$

3.2 The Polarizable Continuum Model

A continuum model in computational molecular sciences can be defined as a model in which a number of the degrees of freedom of the constituent particles (a large number, indeed) are described in a continuous way, usually by means of a distribution function.
In the case of PCM, the problem of molecular solvation is formulated from a classical point of view: a molecule in a solution is represented as a charge density ρ_M due to both point charges and a continuous density, inside a cavity C of proper shape and dimension, within a continuous polarizable medium (the dielectric characterized by the electric permittivity ϵ).[39] The charge distribution ρ_M of the solute, inside the cavity, polarizes the dielectric continuum, which in turn polarizes the solute charge distribution. This definition of the interaction corresponds to a self-consistent process, which is numerically solved following an iterative procedure.
We will first consider the electrostatic problem, which will then be nested into the QM framework. The general Poisson equation[40]

$$-\vec{\nabla} \cdot [\epsilon(r)\vec{\nabla} \cdot \vec{V}(r)] = 4\pi\rho_M(r) \tag{3.63}$$

can be semplified to

$$-\nabla^2 V_M(r) = 4\pi\rho_M(r) \ , \ for \ r \in C \tag{3.64}$$

$$-\epsilon\nabla^2 V(r) = 0 \ , \ for \ r \in C \notin C \tag{3.65}$$

We can then define the reaction potential $V(r)$:

$$V(r) = V_M(r) + V_R(r) \tag{3.66}$$

From a pratical point of view, it is also very important to define a set of boundary conditions at the cavity surface Γ[41]:

$$\begin{cases} [V] = cost \ on \ \Gamma \\ [\partial V] = 0 \ on \ \Gamma \end{cases} \tag{3.67}$$

The first jump condition expresses the continuity of the potential across the surface, whereas the second one involves the continuity of the component of the field (expressed as the gradient of V) that is perpendicular to the cavity surface:

$$[\partial V] = (\frac{\partial V}{\partial \vec{n}})_{in} - \epsilon(\frac{\partial V}{\partial \vec{n}})_{out} \tag{3.68}$$

where $\vec{n}$ is the outward-pointing vector perpendicular to the cavity surface.
All the equations above represent the electrostatic foundation needed to define the problem. It is now necessary to illustrate one of the possible approaches to its solution: the apparent surface charge (ASC) method, where an apparent surface charge density $\sigma(s^2)$ is spread on the cavity surface Γ. The ASC defines a reaction potential over the whole space, which is equivalent to the reaction potential V_R:

$$V_\sigma(r) = \int_r \frac{\sigma(\vec{s})}{|\vec{r} - \vec{s}|} \tag{3.69}$$

The integration of equation 3.69 is computationally challenging, especially over a surface of irregular shape. Therefore, it is often discretized into a number of finite elements to be solved numerically. The cavity surface is approximated in terms of a set of finite elements (called *tesserae*) small enough to consider $\sigma(\vec{s})$ almost constant within each tessera (the area of which is A_k). Therefore:

$$q_k = \sigma(\vec{s_k})A_k \tag{3.70}$$

$$V_\sigma(r) \approx \sum_k^{Nts} \frac{\sigma(\vec{s_k})A_k}{|\vec{r} - \vec{s_k}|} = \sum_k^{Nts} \frac{q_k}{|\vec{r} - \vec{s_k}|} \tag{3.71}$$

Where the q_ks are the point charges in terms of the local value of $(\vec{s_k})$ on each tessera. The local value of the potential necessary to define q_k also depends on the whole set of the surface charges, and so the correct values of the surface charges, and the correct expression of the reaction potential, are to be obtained through an iterative procedure.
Based on the definition of q_k we can distinguish different formulations of PCM, that have been developed over the years: DPCM[41], IEFPCM[42] and CPCM[43]. All of the above formulations, however, share common features that we will be considering here.
Equation 3.70 is rewritten in matrix form:

$$\mathbf{q} = \text{-}\mathbf{Q}\mathbf{f}_M \tag{3.72}$$

$\mathbf{Q}$ is a square matrix NTs x NTs collecting cavity geometrical factors ($\vec{s_k}$ and A_k for each tessera) and the dielectric constant of the medium; $\mathbf{q}$ and $\mathbf{f}_M$ are column matrices, the first containing the unknown charges and the second the values of the proper electrostatic quantity, namely, the normal component of the solute electric field or the solute electrostatic potential, calculated at the tesserae. Here we present the definition of $\mathbf{Q}$ and $\mathbf{f}$ for the IEFPCM and CPCM formulation:

version	**Q**	**f**
CPCM	$\mathbf{S}^{-1}$	$\mathbf{V}_M$
IEFPCM	$[(2\pi\frac{\epsilon+1}{\epsilon-1}\mathbf{A}^{-}1-\mathbf{D}^{*})\mathbf{S}]^{-1}(2\pi\mathbf{A}^{-1}-\mathbf{D})$	V_M

where $\mathbf{A}$ is the diagonal matrix of tesserae areas and $\mathbf{S}$ and $\mathbf{D}$:

$$\begin{cases} S_{ii} = 1.0694\sqrt{\dfrac{4\pi}{a_i}} \\ S_{ij} = \dfrac{1}{|\vec{s_i} - \vec{s_j}|} \end{cases} \tag{3.73}$$

$$\begin{cases} D_{ii} = -(2\pi + \displaystyle\sum_{i \neq j} D_{ij} a_j)\frac{1}{a_i} \\ D_{ij} = \dfrac{(\vec{s_i} - \vec{s_j}) \cdot \hat{\mathbf{n}}_j}{|\vec{s_i} - \vec{s_j}|^3} \end{cases} \tag{3.74}$$

where a_i is the area of tessera i.

QM framework

Now that we have presented the electrostatic backbone of the method, we should translate PCM equations in quantum mechanical language, resorting to the concept of focused models. In fact, we will define an effective hamiltionian for the solute-solvent system:

$$\hat{H_{eff}} = \hat{H_0^M} + \hat{V^{int}} \tag{3.75}$$

where $\hat{H_0^M}$ is the Hamiltonian of the solute, the focused part of the model, and $\hat{V}^{int}$ (the solvent reaction potential) represents the solute-solvent interaction. From here on, we are assuming valid the Born-Oppenheimer approximation and will therefore divide the charge distribution into its nuclear and electronic component:

$$\rho_M(r) = \rho_M^e(r) + \rho_M^e \tag{3.76}$$

Only the electronic term of equation 3.76 is effectively modified, with respect to the initial guess, by $\hat{V}^{int}$. $\hat{V}^{int}$ itself changes through the iterative cycle. Such operator can be divided into four terms having similarities with the two-, one- and zero-electron terms present in the solute Hamiltonian. It is however more intuitive to show these similarities in the definition of the interaction energy U_{int} given as the integral of the reaction potential times the whole charge distribution ρ_M:

$$U^{int} = U^{ee} + U^{en} + U^{ne} + U^{nn} \tag{3.77}$$

where U^{xy} corresponds to the interaction energy between the component of the interaction potential having as source ρ_M^x, namely $\hat{V}_{int}^x$, and the charge distribuition ρ_M^y.

Now the Schrödinger equation has to be solved in the variational framework:

$$\hat{H}_{eff}|\Psi\rangle = E|\Psi\rangle \tag{3.78}$$

It can be demonstrated that the functional one has to minimize to reach a sensible solution is the free energy functional shown in eq 3.79 . This demonstration, however, exceeds the purpose of this thesis: we will therefore simply consider this fact as a statement from here on.

$$G = \langle\Psi|\hat{H}^0 + \hat{V}_\sigma|\Psi\rangle - \frac{1}{2}\langle\Psi|\hat{V}_\sigma|\Psi\rangle \tag{3.79}$$

In a self-consistent field (SCF) approach to the problem, either Hartree-Fock or Kohn-Sham, the minimization of G is carried through a Fock operator, defined as the sum of the isolated molecule operator (which can, as usual, be expressed in the basis of molecular orbitals) and the perturbation:

$$\hat{F} = \hat{F}^0 + \hat{V}_\sigma \tag{3.80}$$

where

$$\hat{V}_\sigma = \sum_{k=1}^{Nts} \hat{V}_k q_k \quad \text{and} \quad \hat{V}_k = -\frac{1}{|r - s_k|} \tag{3.81}$$

The point charges q_ks represent the solution of the PCM iterative problem. As discussed before, their definition changes according to the formulation one is considering. In the IEF:

$$q_k = \sum_{l=1}^{Nts} Q_{kl} V_l \qquad k, l \to s_k, s_l \tag{3.82}$$

where V_l are the expectation values (including nuclear contributions) of the electrostatic potential operator computed on the surface element s_l:

$$V_l^e + V_l^N uc = -\sum_i^{occ} \int \phi_i^*(r)\phi_i(r)\frac{1}{|r - s_l|}dr + \int \rho^{Nuc}(r)\frac{1}{|r - s_l}|dr \tag{3.83}$$

Therefore, in this formalism, one can rewrite equation 3.79, for the ground state of the solvated system, as:

$$G_{GS} = \langle\Psi_{GS}|\hat{H}^0 + \hat{V}_\sigma|\Psi_{GS}\rangle - \frac{1}{2}\langle\Psi_{GS}|\hat{V}_\sigma|\Psi_{GS}\rangle = E^{GS} - \frac{1}{2}\sum_k V_k^{GS} q_k^{GS} \tag{3.84}$$

3.3 Polarization response after excitation

Whenever the solute charge distribuition changes as a consequence of a time-dependent process, the microscopic components (electrons, atoms, molecules) that constitute the solvent will take a definite amount of time, referred to as characteristic time for each class of particles, to reach a certain equilibrium of the polarization. If the characteristic times of the solvent are of the same order of magnitude as the period required for an appreciable change of the solute charge distribuition, then the solvent response will not be sufficiently rapid to build up a new equilibrium polarization, and the actual value of the polarization will lag behind the changing charge distribution. The expression for the total polarization is, in the domain of frequencies:

$$\vec{P}(\omega) = \frac{\hat{e}(\omega - 1)}{4\pi}\vec{E}(\omega) \tag{3.85}$$

Here, the dielectric permittivity

$$\hat{e}(\omega) = e^{'}(\omega) - ie^{''}(\omega) \tag{3.86}$$

is a complex variable: the real component is in phase with the oscillating field and the complex part, or loss factor, is perpendicular to the Maxwell field and generates a loss of energy of the electric field in the medium.
In general, the behavior of polar compounds in an electromagnetic fields is built up of three parts: the orientational, the nuclear and the electronic polarization. Each component presents a different CT and therefore the orientational contribuitions will first start to lag behind the variations of the electromagnetic field, followed by the nuclei and then by the electrons. However, it is resonable to make the following approximation and spilt the total polarization in two terms only:

$$\vec{P}(t) \approx \vec{P}_{fast} + \vec{P}_{slow} \tag{3.87}$$

In general, the fast term refers to the part of the solvent response that always follows the dynamics of the process and slow refers to the remaining inertial term, however the specific degrees of freedom associated with each partition depend on the phenomenon one is observing. For instance, when considering vertical electronic transitions, the only contribuition to $\vec{P}_{fast}$ comes from the response of the solute electrons. This partition of the polarization vector of the medium gives rise to what is called a "nonequilibrium" regime. By contrast, one refers to the "equilibrium" solvation when the $\vec{P}_{slow}$ is virtually equal to zero and therefore all the degrees of freedom of the solvent are given sufficient time to respond to the change of the charge distribuition of the solute.

3.3.1 PCM-Linear Response

The equation given in the previous section 3.84 now needs to be generalised for excited states, both in the equilibrium and the nonequilibrium regime.

Equilibrium

In the case of equilibrium solvation, we will assume that the solvent reaction field has had time to completely relax from the initial ground state value to a new solute-solvent equilibrium. If we indicate the generic excited state with the letter K[44]:

$$\hat{V}_\sigma^{GS} \leftarrow \hat{V}_\sigma^K \tag{3.88}$$

We also have to formulate an expression for free energy in this regime: we will consider an excited state energy in equilibrium with a ground-state solvent reaction field.

$$\begin{aligned} E_{GS}^{K,eq} &= \langle \Psi_{eq}^K | \hat{H}^0 + \hat{V}_\sigma^{GS} | \Psi_{eq}^K \rangle \\ &= \langle \Psi_{eq}^K | \hat{H}^0 | \Psi_{eq}^K \rangle + \sum_l^{Nts} \langle \Psi_{eq}^K | \hat{V}_l q_l^{GS} | \Psi_{eq}^K \rangle \\ &= \langle \Psi_{eq}^K | \hat{H}^0 | \Psi_{eq}^K \rangle + \sum_l^{Nts} V_l^K q_l^{GS} \end{aligned} \tag{3.89}$$

Here we consider the PCM definition of the reaction potential given in eq 3.92 and the IEF formulation to calculate point charges:

$$q_l^{GS} = \sum_{m=1}^{Nts} Q_{lm} V_m^{GS} = \sum_{m=1}^{Nts} Q_{lm} \langle \Psi^{GS} | \hat{V}_m | \Psi^{GS} \rangle \tag{3.90}$$

As we discussed above, the functional one has to minimize in the PCM framework is the free energy, whose expression can be written as follows:

$$G_{eq}^K = \langle \Psi_{eq}^K | \hat{H}^0 + \frac{1}{2} \hat{V}_\sigma^K | \Psi_{eq}^K \rangle = E_{GS}^{K,eq} - \sum_l^{Nts} V_l^K q_l^{GS} + \frac{1}{2} \sum_l^{Nts} V_l^K q_l^K \tag{3.91}$$

Now, if we partition the excited state density matrix in two terms, therefore describing it as the grounds state density matrix corrected for an excitation contribuition, V_l^k and q_l^k can be rewritten as:

$$V_l^k = V_l^{GS} + V_l^\Delta \quad \text{and} \quad q_l^k = q_l^{GS} + q_l^\Delta \tag{3.92}$$

The work equation, whose solution we get through the iterative procedure, therefore is:

$$G_{eq}^{K} = E_{GS}^{K,eq} - \frac{1}{2}\sum_{l}^{Nts} V_l^{GS} q_l^{GS} + \frac{1}{2}\sum_{l}^{Nts} V_l^{\Delta} q_l^{\Delta} \tag{3.93}$$

Both at a theoretical level, in the limit of an exact solution of the electrostatic problem, and through computational test we can safely assume the following equivalence in relation to eq.3.93:

$$V_l^{GS} q_l^{\Delta} = V_l^{\Delta} q_l^{GS} \tag{3.94}$$

Nonequilibrium

In the case of nonequilibrium solvation, point charges referring to the ground state system need to be partitioned into two components, a dynamic and an inertial part

$$q_l^{M} = \sum_{f}^{Nts} Q_{fl}(\epsilon) V_f^{M} \tag{3.95}$$

$$q_l^{M,dyn} = Q_{fl}(\epsilon_\infty) V_f^{M} V_f^{M} \tag{3.96}$$

$$q_l^{M,in} = q_l^{M} - q_l^{M,dyn} \tag{3.97}$$

where M is a generic state of the solute and ϵ_∞ the optical dielectric constant of the solvent. If the state M is described by the wavefunction Ψ_K^{neq}, we can reformulate the expression above in this form:

$$q_l^{K,in} = q_l^{GS,in} = \sum_{f} Q_{fl}(\epsilon) V_l^{GS} - \sum_{f} Q_{fl}(\epsilon_\infty) V_l^{GS} \tag{3.98}$$

$$q_l^{K,dyn} = \sum_{f} Q_{fl}(\epsilon_\infty) V_l^{K} = \sum_{f} Q_{fl}(\epsilon_\infty) V_l^{GS} + \sum_{f} Q_{fl}(\epsilon_\infty) V_l^{\Delta neq,e} \tag{3.99}$$

The meaning of $V_l^{\Delta neq,e}$ is again associated with the partition of the excited state density matrix we had already described in the equilibrium regime.

In light of the new definition of the point charges, one can also write an expression for the nonequilibrium excited state energy in the presence of the ground state reaction field

$$E_{GS}^{K,neq} = \langle \Psi_{neq}^{K} | \hat{H}^0 + \hat{V}_\sigma^{GS} | \Psi_{neq}^{K} \rangle = \langle \Psi_{neq}^{K} | \hat{H}^0 | \Psi_{neq}^{K} \rangle + \sum_{l}^{Nts} V_l^{K,neq} [q_l^{GS,in} + q_l^{GS,dyn}] \tag{3.100}$$

as well as an expression of the free energy

$$G_k^{neq} = \langle \Psi_{neq}^K | \hat{H}^0 + \hat{V}_\sigma^{GS,in} + \hat{V}_\sigma^{K,dyn} | \Psi_{neq}^K \rangle + \tag{3.101}$$

$$-\frac{1}{2}\langle \Psi_{GS} | \hat{V}_\sigma^{GS,in} | \Psi_{GS} \rangle - \frac{1}{2}\langle \Psi_K^{neq} | \hat{V}_\sigma^{K,dyn} | \Psi_K^{neq} \rangle \tag{3.102}$$

$$= E_{GS}^{K,neq} - \frac{1}{2}\sum_l^{Nts} V_l^{GS} q_l^{GS} + \frac{1}{2}\sum_l^{Nts} V_l^{\Delta,neq} q_l^{\Delta,neq} \tag{3.103}$$

if we consider true the approximation show in equation 3.94. Finally, we are able to obtain a systematic definition of the vertical transition energy for solvated systems, by subtracting the ground state free energy from equation 3.84 from the values one gets from equations 3.93 and 3.103 :

$$\omega_K^{eq} = G_k^{eq} - G_{GS} = \Delta E_{GS}^{K0,eq} + \frac{1}{2}\sum_l^{Nts} V_l^{\Delta} q_l^{\Delta,dyn} \tag{3.104}$$

$$\omega_K^{eq} = G_k^{eq} - G_{GS} = \Delta E_{GS}^{K0,neq} + \frac{1}{2}\sum_l^{Nts} V_l^{\Delta,neq} q_l^{\Delta neq,dyn} \tag{3.105}$$

The Linear Response (LR) approach to the problem we just described makes it possible to solve in a single step calculation the entire spectrum of the excited states of interest, both in the equilibrium and nonequilibrium formulation, in contrast to a state-specific method, which would require a two-step calculation for the nonequilibrium regime.
The problem can be formulated in accordance with KS-LR (Eq.3.48)[44, 45]:

$$\begin{bmatrix} \mathbf{A} & \mathbf{B} \\ \mathbf{B*} & \mathbf{A*} \end{bmatrix} \begin{bmatrix} \mathbf{X} \\ \mathbf{Y} \end{bmatrix} = \omega \begin{bmatrix} \mathbf{1} & \mathbf{0} \\ \mathbf{0} & \mathbf{-1} \end{bmatrix} \begin{bmatrix} \mathbf{X} \\ \mathbf{Y} \end{bmatrix} \tag{3.106}$$

In this formalism, the meaning of the elements of matrix **A** and **B** is:

$$\begin{aligned} A_{ia\sigma,jb\tau} = \delta_{ij}\delta_{ab}\delta_{\sigma\tau}(\epsilon_a - \epsilon_b) + \langle i_\sigma j_\tau | a_\sigma b_\tau \rangle + \\ -C_{HF}\delta_{\sigma\tau}\langle i_\sigma a_\sigma | j_\tau b_\tau \rangle + \\ +(1 - C_{HF})\langle i_\sigma j_\tau | f_{xc} | a_\sigma b_\tau \rangle + \nu_{ai,jb}^{PCM} \end{aligned} \tag{3.107}$$

$$\begin{aligned} B_{ia\sigma,jb\tau} = \langle i_\sigma b_\tau | a_\sigma j_\tau \rangle - C_{HF}\delta_{\sigma\tau}\langle i_\sigma a_\sigma | j_\tau b_\tau \rangle + \\ +(1 - C_{HF})\langle i_\sigma b_\tau | f_{xc} | a_\sigma j_\tau \rangle \end{aligned} \tag{3.108}$$

In both definitions, one can see an explicit effect of the solvent (in the perturbation term $\nu_{ai,jb}^{PCM}$) as well as an implicit action (the solvent effectively modifies the molecular orbitals and the corresponding orbital energies, which are in fact solutions

of the Fock equations including solvent reaction terms). The perturbation can be defined, at a qualitative level, as the electrostatic interaction between the charge distribution and the dynamic contribution to the solvent reaction potential induced by the charge distribution:

$$\nu_{ai,jb}^{PCM} = \sum_k V_{ai}(\vec{s}_k) q_{bj}^{dyn} \tag{3.109}$$

If we compare equation 3.105 with equation 3.109, it is clear how the two present a different formal and physical description of the PCM term. In fact, while they both give the same definition of the energy change related to the transition of the molecule from its ground state -in equilibrium with the solvent- to the state K - in the presence of a solvent polarization frozen to the value proper for the solute ground state - namely $\Delta E_{GS}^{K0,neq}$, they diverge in the term associated with the relaxation of the solvent to equilibrate with the charge density of the solute excited state. In fact, the energy variation accompanying this relaxation is not explicitly accounted for in the LR framework. On the contrary, the LR accounts for a correction which, being originated by the dynamic solute-solvent interactions, might be classified as a part of dispersion.[16, 17]

3.3.2 The corrected Linear Response

If we now go back to equations 3.93 and 3.105, we can see that excited-state free energies can be obtained by calculating the frozen-PCM energy (E_{GS}^{K}) and the relaxation term of the density matrix (P^{Δ} or $P^{\Delta,neq}$), where the calculation of the relaxed density matrices requires the solution of a nonlinear problem being the solvent reaction field dependent on such densities.
By introducing a perturbative scheme, truncated at the first order, in the LR framework we can obtain such quantities with a reasonable level of accuracy: this is the corrected Linear Response (cLR) approach, that we will now briefly describe. First of all, we take into account that the LR allows us to obtain an estimate value of the difference between the excited- and ground-state energies in the presence of a frozen ground state solvent ($\Delta E_{GS}^{K0,neq}$) and we can therefore define the equilibrium and nonequilibrium free energies as follows:

$$G_K^{eq} = G_{GS} + \omega_k^0 + \frac{1}{2}\sum_l^{Nts} V_l(P^{\Delta}) q_l^{(\Delta,dyn)} \tag{3.110}$$

$$G_K^{neq} = G_{GS} + \omega_k^0 + \frac{1}{2}\sum_l^{Nts} V_l(P^{\Delta,neq}) q_l^{(\Delta neq,dyn)} \tag{3.111}$$

where the only unknow term is the relaxation part of the density matrix, since ω_k^0 is simply the eigenvalue of the system in presence of the frozen GS solvent, and therefore corresponding apparent charges. A strategy one can use to calculate P^{Δ} for each state K is through the extending LR approaches to analytical energy gradients. The charges, then, can be calculated as:

$$q_l^{\Delta,x} = \sum_m^{Nts} Q_{ml}\epsilon(x)V_m^{\Delta,x} \tag{3.112}$$

$$\begin{cases} \epsilon_x = \epsilon \\ P^{\Delta,x} = P^{\Delta} \\ q_l^{\Delta,x} = q_l^{\Delta} \end{cases} \quad \text{(equilibrium regime)}$$

$$\begin{cases} \epsilon_x = \epsilon_\infty \\ P^{\Delta,x} = P^{\Delta,neq} \\ q_l^{\Delta,x} = q_l^{\Delta,neq} \end{cases} \quad \text{(nonequilibrium regime)} \tag{3.113}$$

By introducing the TD-DFT relaxed density and the corresponding charges (3.112) into (3.81) and (3.82) we obtain the first-order approximation to the exact free energy of the excited state by using a linear response scheme.[46]
The scheme is then implemented by solving twice TD-DFT equations:

a. First, the excitation energies ω_K^0 are computed, leaving out the explicit solvent contribution;

b. Then, these solutions are used as a guess to solve the TD-DFT equations again, but this time the explicit solvent contribution is included and the corresponding relaxed density is computed and used as explained above.

However, it is worth noticing that the largest contribution to the solvatochromic shift comes from the values of the ω_K^0s, which are calculated in the same way both in LR and cLR schemes. Therefore, one can expect that in all cases cLR and the LR approaches will give very similar descriptions of the solvent effect and, in particular, of the relative shift passing from one solvent to the other.

3.3.3 The Vertical Excitation Model

The Vertical Excitation Model represents another possible strategy to introduce a State Specific (SS) correction in the LR approach. In this scheme, a SS reaction field is employed which can be self-consistent with either the unrelaxed (UD, T) or the relaxed density (RD, $P^{\Delta)}$). The method has also been demonstrated to be

variational[47], which facilitates the derivation of energy gradients as we will explain later. In the RD formulation, the solvent polarization response charges depends on the complete ground-to-excited state density difference whereas in the UD, the Z-vector component is not included.[48] If we label the density of an ES by **P**, the relation between the various density matrices are

$$\mathcal{P}_I = \mathcal{P}^{\mathcal{GS}} + \mathcal{P}^{\cdot} = \mathcal{P}^{\mathcal{GS}} + \mathcal{T} + \mathcal{Z}. \tag{3.114}$$

The unrelaxed component T of the ES density P^{Δ} is defined by the eigenvectors of the TD-DFT equations

$$\mathcal{T} = |\mathbf{X}, \mathbf{Y}\rangle + \langle \mathbf{X}, \mathbf{Y}| = \frac{1}{2}|\mathbf{X}+\mathbf{Y}\rangle\langle \mathbf{X}+\mathbf{Y}| + \frac{1}{2}|\mathbf{X}-\mathbf{Y}\rangle\langle \mathbf{X}-\mathbf{Y}| \tag{3.115}$$

where T contains the occupied-occupied and virtual-virtual MO blocks of the ground-to-excited state density matrix P^{Δ}.

$$T_{ij} = -\frac{1}{2}[\sum_a (\mathbf{X}+\mathbf{Y})_{ia}(\mathbf{X}+\mathbf{Y})_{ja} + [\sum_a (\mathbf{X}-\mathbf{Y})_{ia}(\mathbf{X}-\mathbf{Y})_{ja}], \tag{3.116}$$

$$T_{ab} = \frac{1}{2}[\sum_i (X+Y)_{ia}(X+Y)_{ib} + [\sum_b (X-Y)_{ia}(X-Y)_{ib}], \tag{3.117}$$

$$T_{\mu\nu} = \sum_{ij} T_{ij} C_{\mu i} C_{j\nu} \otimes \sum_{ab} T_{ab} C_{\mu a} C_{b\nu} \tag{3.118}$$

The formulation of VEM (in both RD and UD flavors) has been introduced within a Configuration Interaction Singles (CIS) approach, and the equations have been then extended to the TD-DFT framework. In order to show how the VEM correction comes to action, we recall some definitions in the solute-solvent interaction scheme. For a generic one-particle density matrix P in the MO basis, the electrostatic potential at the surface elements is defined as

$$\mathbf{V} = \sum_{pq} V_{pq} = \sum_{pq} P_{pq} \sum_{\mu\nu} C_{\mu p} C_{\nu q} \mathbf{V}_{\mu\nu} = \sum_{\mu\nu} P_{\mu\nu} \mathbf{V}_{\mu\nu}, \tag{3.119}$$

where $V_{\mu\nu}$ is the "uncontracted" contribution from a pair of AOs basis functions on the surface element g, which is expressed as an electrostatic repulsion integral as we use a continuous surface charge distribution

$$V_{\mu\nu,g} = \langle \mu\nu | g \rangle. \tag{3.120}$$

Given the potential, the surface charges are defined as

$$\mathbf{q}[\mathcal{P}] = \mathbf{Q} \sum_{\mu\nu} P_{\mu\nu} \mathbf{V}_{\mu\nu}, \tag{3.121}$$

where the $\mathbf{Q}$ matrix represents the solution of the PCM polarization equations [eq.3.72].
The VEM correction is introduced in the components $\mathbf{A}$ and $\mathbf{B}$ of the electronic Hessian, which is the left-hand side of the non-Hermitian TD-DFT eigensystem,

$$\begin{aligned} A^{\mathrm{VEM}}_{ia,jb} &= A_{ia,jb} + (V_{ab}\delta_{ij} - V_{ij}\delta_{ab})q[T] \\ &= (\epsilon_a - \epsilon_i)\delta_{ij}\delta_{ab} - (ia|jb) + f^{xc}_{ia,jb} - c_X(ab|ij) + (V_{ab}\delta ij - V_{ij}\delta_{ab})q[T] \end{aligned} \tag{3.122}$$

$$\begin{aligned} B^{\mathrm{VEM}}_{ia,jb} &= B_{ia,jb} + (V_{ab}\delta_{ij} - V_{ij}\delta ab)q[T] \\ &= (ia|jb) + f^{xc}_{ia,jb} - cX_{jaib} + (V_{abij} - V_{ijab})q[T]. \end{aligned} \tag{3.123}$$

The generalized eigenvalue problem to be solved has dimension $2N_{\mathrm{occ}}N_{\mathrm{vir}}$ and is defined as

$$\begin{bmatrix} \mathbf{A}^{\mathrm{VEM}} & \mathbf{B}^{\mathrm{VEM}} \\ \mathbf{B}^{\mathrm{VEM}} & \mathbf{A}^{\mathrm{VEM}} \end{bmatrix} \begin{bmatrix} \mathbf{X} \\ \mathbf{Y} \end{bmatrix} = \omega^* \begin{bmatrix} 1 & 0 \\ 0 & -1 \end{bmatrix} \begin{bmatrix} \mathbf{X} \\ \mathbf{Y} \end{bmatrix}, \tag{3.124}$$

where the vectors $|\mathbf{X}, \mathbf{Y}\rangle$ are defined in the same Hilbert space and are normalized as

$$\langle \mathbf{X}, \mathbf{Y}|_K \Delta |\mathbf{X}, \mathbf{Y}\rangle_L = \delta_{KL} \tag{3.125}$$

over the metric

$$\Delta = \begin{bmatrix} 1 & 0 \\ 0 & -1 \end{bmatrix}. \tag{3.126}$$

Given the definitions above, the ES polarization charges depend on the unrelaxed density T only and they are given by

$$\mathbf{q}[\mathcal{T}] = \mathbf{Q}\mathbf{V}[\mathcal{T}] = \mathbf{Q}\langle \mathbf{X}, \mathbf{Y}|(V_{abij} - V_{ijab})|\mathbf{X}, \mathbf{Y}\rangle. \tag{3.127}$$

The dependence of $\mathbf{A}^{\mathrm{VEM}}$ and $\mathbf{B}^{\mathrm{VEM}}$ on $\mathbf{q}[\mathcal{T}]$ makes the eigensystem nonlinear, and therefore it needs to be iteratively solved for any given state, until self-consistency

is achieved

$$\begin{aligned}\omega^* &= \frac{1}{2}\langle \mathbf{X}+\mathbf{Y}|(\mathbf{A}+\mathbf{B})^{\mathrm{VEM}}|\mathbf{X}+\mathbf{Y}\rangle + \frac{1}{2}\langle \mathbf{X}-\mathbf{Y}|(\mathbf{A}-\mathbf{B})|\mathbf{X}-\mathbf{Y}\rangle \\ &= \frac{1}{2}\langle \mathbf{X}+\mathbf{Y}|(\mathbf{A}+\mathbf{B})|\mathbf{X}+\mathbf{Y}\rangle + \frac{1}{2}\langle \mathbf{X}-\mathbf{Y}|(\mathbf{A}-\mathbf{B})|\mathbf{X}-\mathbf{Y}\rangle + \\ &\quad + \langle \mathbf{X}+\mathbf{Y}|(\mathbf{V}_{ab}\delta_{ij}-\mathbf{V}_{ij}\delta_{ab})|\mathbf{X}+\mathbf{Y}\rangle \mathbf{q}[\mathcal{T}]\end{aligned} \tag{3.128}$$

At the first iteration, the eigenvalues can be written as

$$\omega^* = \omega_0 + \langle \mathbf{X}+\mathbf{Y}|(\mathbf{V}_{ab}\delta_{ij}-\mathbf{V}_{ij}\delta_{ab})|\mathbf{X}+\mathbf{Y}\rangle \mathbf{q}[\mathcal{T}], \tag{3.129}$$

where ω_0 represents the excitation energy affected by the solvent polarization of the ground state only, i.e., the effect of the solvent reaction field is only indirectly taken into account through the MOs and the orbital energies calculated for the GS. At convergence on the nonlinear solution, the quantity ω is used to evaluate the state-specific VEM-UD excitation energy as

$$\omega^{\mathrm{VEM}} = \omega^* - \frac{1}{2}\langle \mathbf{X}+\mathbf{Y}|(\mathbf{V}_{ab}\delta_{ij}-\mathbf{V}_{ij}\delta_{ab})|\mathbf{X}+\mathbf{Y}\rangle \mathbf{q}[\mathcal{T}]. \tag{3.130}$$

We can now move on to the derivation of the analytical gradients of VEM-UD energy, thanks to the already mentioned variational character of the Lagrangian formulation.

Analytical gradients of VEM-UD energy

Since ω^* is, at convergence, the stationary point of the VEM-UD variational free excitation energy functional defined as

$$\begin{aligned}\omega^{\mathrm{VEM}} =& \mathcal{G}\left[\mathbf{X},\mathbf{Y},\omega^*\right] \\ =& \langle \mathbf{X},\mathbf{Y}|\mathbf{\Lambda}|\mathbf{X},\mathbf{Y}\rangle + \frac{1}{2}\left\langle \mathbf{X},\mathbf{Y}\left|\mathbf{\Lambda}^{\mathrm{VEM}}\right|\mathbf{X},\mathbf{Y}\right\rangle \mathbf{q}[\mathcal{T}] \\ & - \omega^*(\langle \mathbf{X},\mathbf{Y}|\Delta|\mathbf{X},\mathbf{Y}\rangle - 1)\end{aligned} \tag{3.131}$$

with

$$\mathbf{\Lambda} = \begin{bmatrix} \mathbf{AB} \\ \mathbf{BA} \end{bmatrix} \tag{3.132}$$

$$\mathbf{\Lambda}^{\mathrm{VEM}} = \begin{bmatrix} (\mathbf{V}_{ab}\delta_{ij}-\mathbf{V}_{ij}\delta_{ab})\,(\mathbf{V}_{ab}\delta_{ij}-\mathbf{V}_{ij}\delta_{ab}) \\ (\mathbf{V}_{ab}\delta_{ij}-\mathbf{V}_{ij}\delta_{ab})\,(\mathbf{V}_{ab}\delta_{ij}-\mathbf{V}_{ij}\delta_{ab}) \end{bmatrix} \tag{3.133}$$

In the presence of an external perturbation ξ , such as a nuclear coordinate or a component of an external electric field, we can write

$$\begin{aligned}\mathcal{G}^{(\xi)}\left[\mathbf{X},\mathbf{Y},\omega^*\right] = &\left\langle \mathbf{X},\mathbf{Y}\left|\mathbf{\Lambda}^{(\xi)}\right|\mathbf{X},\mathbf{Y}\right\rangle \\ &+\frac{1}{2}\left\langle \mathbf{X},\mathbf{Y}\left|\mathbf{\Lambda}^{\mathrm{VEM}(\xi)}\right|\mathbf{X},\mathbf{Y}\right\rangle \mathbf{q}[\mathcal{T}] \\ &+\frac{1}{2}\left\langle \mathbf{X},\mathbf{Y}\left|\mathbf{\Lambda}^{\mathrm{VEM}}\right|\mathbf{X},\mathbf{Y}\right\rangle \mathbf{q}^{(\xi)}[\mathcal{T}]\end{aligned} \tag{3.134}$$

We can now use the Z-vector method described by eq.3.57 to solve for a single perturbation, irrespective of how many external perturbations are considered. This approach allows us to avoid the calculation of the the derivatives of the MO coefficients with respect to each external perturbation. We have to consider the extended Lagrangian:

$$\mathcal{L}\left[\mathbf{X},\mathbf{Y},\omega^*,\mathbf{C},\mathbf{Z},\mathbf{W}\right] = \mathcal{G}\left[\mathbf{X},\mathbf{Y},\omega^*\right] + \sum_{ia} Z_{ia}F_{ia} - \sum_{pq,p\leq q} W_{pq}\left(S_{pq}-\delta_{pq}\right) \tag{3.135}$$

The derivatives with respect to the Z-vector Z_{ia} ensure that the SCF conditions remain satisfied

$$\frac{\partial \mathcal{L}}{\partial Z_{ia}} = F_{ia} = 0 \tag{3.136}$$

and the MOs that satisfy theKS equations are constrained to be orthonormal, which is ensured by the Lagrangian multiplier W_{pq}:

$$\frac{\partial \mathcal{L}}{\partial W_{pq}} = S_{pq} - \delta_{pq} = 0 \tag{3.137}$$

Both Z_{ia} and W_{pq} are determined from the condition

$$\frac{\partial \mathcal{L}}{\partial C_{\mu p}} = 0 \tag{3.138}$$

Then the derivatives of the excitation energy are

$$\omega^{\mathrm{VEM}(\xi)} = \mathcal{L}^{(\xi)}\left[\mathbf{X},\mathbf{Y},\omega^*,\mathbf{C},\mathbf{Z},\mathbf{W}\right] = \mathcal{G}^{(\xi)}\left[\mathbf{X},\mathbf{Y},\omega^*\right] + \sum_{ia} Z_{ia}F_{ia}^{(\xi)} - \sum_{pq,p\leq q} W_{pq}S_{pq}^{(\xi)} \tag{3.139}$$

SCF condition remains satisfied if $\mathbf{X},\mathbf{Y},\omega^*,\mathbf{C},\mathbf{Z}$ and $\mathbf{W}$ have been determined from the stationarity conditions.

Chapter 4

Benchmarking of the method

Here we illustrate the preliminar phase of the study. An initial screening of the substrates was carried at the TD-DFT level with the M06-2X functional to allow for a comparison between different excited-state PCM frameworks (LR, cLR and VEM). Then we defined a new expression for S_1 and T_1 adiabatic solvated energies at using double-hybrid TD-DFT to describe the doubly-excited character of the state. Then, in order to benchmark the method, we compared the resulting ΔE_{ST} with multiconfigurational estimates. Lastly, we also calculated **ss-pol+disp** vertical energies in order to estimate the impact of the adiabatic correction and solvent equilibration on the ΔE_{ST}.

4.1 Computational details

In this phase of the study, all the calculations were performed with the Gaussian16 software package, also resorting to local implementations for VEM and double-hybrid/TD-DFT calculations.[49]
S_0 states were first optimised at DFT/B3LYP/cc-pvtz level *in vacuo* and using PCM for toluene and acetonitrile solvation, since several examples from literature show the reliability of the method for ground state geometries.[50, 51] Appendix A contains data from a preliminary screening on heptazine aimed at determining the effect of the basis set and functional on the vertical excitation energies.
Single point M06-2X/LR-PCM, M06-2X/cLR-PCM and M06-2X/VEM-PCM (in toluene and acetonitrile) calculations were carried on those structures using def2-TZVP basis set, as commonly done for excited state geometries.[52, 53]
S_1 and T_1 equilibrium structures were then obtained in gas phase at M06-2X/def2-TZVP and in toluene and acetonitrile using LR-PCM. Since in the LR framework we are able to verify the validity of the minimum through the frequency calculation, we used LR minima as starting point for VEM geometry optimizations. Moreover, we

also reoptimised ground-states structures using M06-2X and the def2-TZVP basis set. The choice was motivated by the need to have the gradients and Hessians of the ground state and excited states obtained at the same level of calculation
Double-hybrid-TD-DFT calculations were carried out in two steps to get around the absence of any implementation of double-hybrids gradients in the TD-DFT framework.
First, S_1 and T_1 geometries were optimised with the def2-TZVP basis set and a modified BLYP exchange-correlation functional, herein named BLYP53, which contains the same amount of Hartree-Fock exchange as the double-hybrid B2PLYP (53%).[54] Structures were obtained *in vacuo*, acetonitrile and toluene (LR-PCM,VEM-PCM). Then, single point TD-DFT energies were computed on each minimum with B2PLYP and the def2-TZVP basis set to correct the adiabatic energy. The only solvation model implemented for this specific type of calculation is LR-PCM.
Finally, for the sake of completeness, we also performed single-point B2PLYP/def2-TZVP and BLYP53/def2-TZVP energy calculations on M06-2X/def2-TZVP geometries, to calculate vertical ΔE_{ST}s.

4.2 Results and Discussion

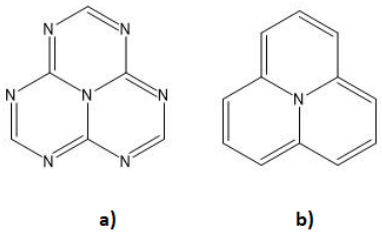

Figure 4.1: Structures of the IST substrates: heptazine (a) and cyclazine (b)

Before presenting the numerical results, let us make some qualitative considerations on the nature of the first singlet and triplet excited states of the systems shown in figure 4.1.

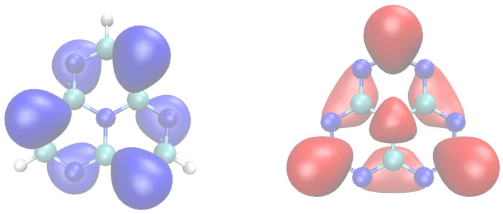

Figure 4.2: Plot of the HOMO and LUMO of heptazine with an isovalue of 0.02 a.u

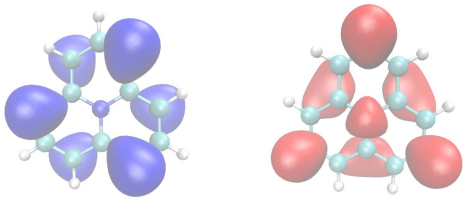

Figure 4.3: Plot of the HOMO and LUMO of cyclazine with an isovalue of 0.02 a.u

Figures 4.2 and 4.3 show the isosurfaces of the highest occupied molecular orbital (HOMO) and lowest unoccupied molecular orbital (LUMO), which also represent the dominant pair of natural transition orbitals (NTOs)[55] for both S_1 and T_1. These systems present a transition from the ground state to the first singlet and triplet of the $\pi \rightarrow \pi^*$ kind, with null oscillator strength and almost pure HOMO-LUMO character. The spatial separation between the frontier orbitals indicates that the exchange interaction is weak, remarking the necessity to include double-excitations to predict a negative ΔE_{ST}. Moreover, the significant spatial separation between HOMO and LUMO points to a potential dominant charge-transfer (CT) character of the transition: the electronic charge is transferred from the peripheral nitrogen atoms to the carbon atoms and the central nitrogen atom.
The CT character of many TADF emitters has been extensively investigated[56–58] and can be and can be assessed, as already shown by Moral et al.[59], using diagnostic tools for TD-DFT. To this regard, a particularly useful parameter is Δr[60], which describes the average hole-electron distance upon excitation.

Heptazine					
Solvent (VEM-PCM)	$\vec{S}$	Φ_i'	Φ_a'	λ_{ia}	NTO $\Delta r(\mathring{A})$
TOL	0	44	45	0.97943	0.01052
TOL	1	44	45	0.97327	0.01782
ACN	0	44	45	0.97831	0.01032
ACN	1	44	45	0.97191	0.01735
Cyclazine					
Solvent (VEM-PCM)	$\vec{S}$	Φ_i'	Φ_a'	λ_{ia}	NTO $\Delta r(\mathring{A})$
TOL	0	44	45	0.99762	0.00389
TOL	1	44	45	0.99754	0.00559
ACN	0	44	45	0.99757	0.00374
ACN	1	44	45	0.99774	0.00557

Table 4.1: NTO character and metrics of $S_0 \rightarrow S_1$ and $S_0 \rightarrow T_1$ transitions at TD-DFT/M06-2X/def2-TZVP

As table 4.1 shows, given the disjoint nature of HOMO and LUMO but the relatively small values of Δr, we can attribute a short-range charge transfer-character to the transition.[4]

4.2.1 Initial screening of the solvation models

We previously discussed that standard TD-DFT is inadequate for the prediction of a negative ΔE_{ST}. However, an initial screening of solvent influence on excited singlets and triplets was made at this level of theory. The results are presented here.

Heptazine				
		S_1		T_1
in vacuo		3.132		3.255
		S_1		T_1
	TOL	ACN	TOL	ACN
ω_0	3.186	3.255	2.970	3.038
LR-PCM	3.184	3.255	2.970	3.038
cLR-PCM	3.182	3.251	2.965	3.033
VEM-PCM	3.174	3.247	2.959	3.030

Table 4.2: Heptazine vertical absorption energies (in eV) at TD-DFT/M06-2X/def2-TZVP

Cyclazine				
		S_1		T_1
in vacuo		1.261		1.070
		S_1		T_1
	TOL	ACN	TOL	ACN
ω_0	1.265	1.265	1.074	1.077
LR-PCM	1.265	1.265	1.074	1.077
cLR-PCM	1.262	1.263	1.068	1.072
VEM-PCM	1.259	1.260	1.062	1.067

Table 4.3: Cyclazine vertical absorption energies (in eV) calculated at TD-DFT/M06-2X/def2-TZVP

The meaning of ω_0 has already been clarified (see paragraph 3.3.3) and will herein be often used a reference parameter.
One can see how the different solvent descriptions produce very similar shifts in the transition values for both substrates from the results listed in Tables 4.2,4.3. However, the state-specif correction introduced in the VEM description clearly induces a higher stabilisation of the excited states (Table 4.4).

	heptazine	**cyclazine**
$\Delta_{\text{LR-}\omega_0}$	0.000	0.000
$\Delta_{\text{cLR-}\omega_0}$	-0.004	-0.005
$\Delta_{\text{VEM-}\omega_0}$	-0.008	-0.010

Table 4.4: Absorption energy shifts (in eV) induced by different solvation models at TD-DFT/M06-2X/def2-TZVP

We also report solvatochromic shift values (Table 4.5, 4.6) for both solvents, treated with each model. As expected, an increase in the polarity of the solvents effectively produces an hypsocromic shift of the absorption wavelenghts.

heptazine	S_1		T_1	
	TOL	ACN	TOL	ACN
Δ_{ω_0}	0.201	0.456	0.201	0.456
Δ_{LR}	0.148	0.334	0.147	0.334
Δ_{cLR}	0.151	0.337	0.147	0.334
Δ_{VEM}	0.158	0.341	0.152	0.339

Table 4.5: Heptazine solvatochromic shifts (in eV) at TD-DFT/M06-2X/def2-TZVP with different solvation models

cyclazine	S_1		T_1	
	TOL	ACN	TOL	ACN
Δ_{ω_0}	0.059	0.133	0.059	0.133
Δ_{LR}	0.059	0.133	0.059	0.133
Δ_{cLR}	0.059	0.131	0.055	0.126
Δ_{VEM}	0.062	0.134	0.061	0.131

Table 4.6: Cyclazine solvatochromic shifts (in eV) at TD-DFT/M06-2X/def2-TZVP with different solvation models

4.2.2 Triplet excited state solvation

The most notable evidence we gathered from the set of data presented so far concerns T_1 energies. In fact, if the solvation model of choice is the LR-PCM, excitation energies are exactly equal to the ω_0 value. This can be easily derived from the theoretical background given in section 3.3.1. Since the $S_0 \rightarrow T_1$ transition density is zero out of spin simmetry, the response of the environment to the excitation in equally null.

Some additional single point energy calculations on small substrates were performed to prove this conclusion. The systems were chosen in accordance with other studies benchmarking triplet excited states calculations [61]. In general the polarization effect on the excitation energy is far more prevalent than the dispersion contribution for polar substrates. For these system, the difference in excited state energies between the LR and the VEM solvation model is larger and can also be appreciated in the singlet energies as shown in table 4.7 and figure 4.4.

	TOL					
molecule	S_1			T_1		
	ω_0	LR-PCM	VEM-PCM	ω_0	LR-PCM	VEM-PCM
acetone	4.151	4.147	4.093	3.688	3.688	3.629
piridina	5.012	5.002	4.877	4.400	4.400	4.270
acetamide	5.555	5.552	5.446	5.126	5.126	5.018
benzochinone	2.703	2.702	2.680	2.303	2.303	2.279
formaldeide	3.770	3.764	3.706	3.238	3.238	3.175
furano	6.732	6.627	6.723	4.391	4.391	4.382
imidazolo	7.016	6.997	6.820	4.950	4.950	4.930
pirrolo	7.024	6.921	7.013	4.756	4.756	4.743
propanamide	5.608	5.606	5.503	5.209	5.209	5.105
stetrazina	2.257	2.254	2.253	1.664	1.664	1.652

Table 4.7: Vertical S_1 and T_1 energies at TD-DFT/M06-2X/6-31+G*

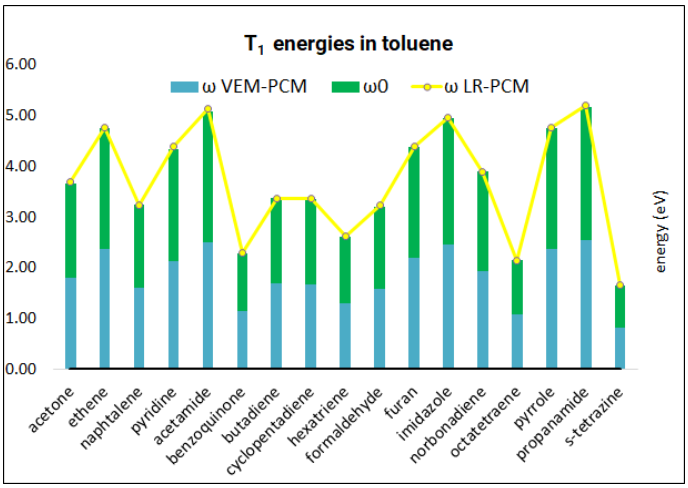

Figure 4.4: Plot of T_1 energies (in eV) in toluene at M06-2X/6-31+G*. VEM energies are represented with blue bars, ω_0 energies are shown in green, LR values are represented with yellow markers

What emerges from this section of the study is the unphysical lack of stabilisation provided by LR-PCM to excited triplets, that makes the framework unsuitable for the study of IST systems.

4.2.3 Geometry optimization

In order to calculate adiabatic singlet-triplet gaps it is necessary to perform excited-state geometry optimizations. In a recent study Jacquemin et al.[11] reported that a EOM-CCSD optimization *in vacuo* of heptazine S_1 starting from the ground state planar D_{3h} geometry leads to the puckering of the central nitrogen atom, with the true minimum therefore exhibiting a C_{3v} point group symmetry. In the same study, the lowest triplet was instead assigned two genuine minima at the UCCSD/cc-pVDZ level. One belongs to the C_{3v} group in analogy with the singlet, while the other exhibits an in-plane deformation that leads to a C_s geometry.
At our level of calculation, we came to analogous results for the lowest excited singlet, not only in gas phase but also in both solvents: the D_{3h} structure presents an imaginary frequency associated with the puckering of the central nitrogen and therefore the true minimum has in fact C_{3v} symmetry. The lowest triplet, on the other hand, only exhibited one imaginary negative frequency associated to the plane distortion at the (LR-PCM)/TD-DFT/M06-2X/def2-TZVP level and is therefore assigned to the C_s symmetry group.

The change of XC-functional from M06-2X to BLYP53 results in an effect worth highlighting, particularly on the singlet structure, although it will be later proved not crucial for our discussion. The optimizations performed with the BLYP53 functional generally produce more planar structures, with the central nitrogen atom

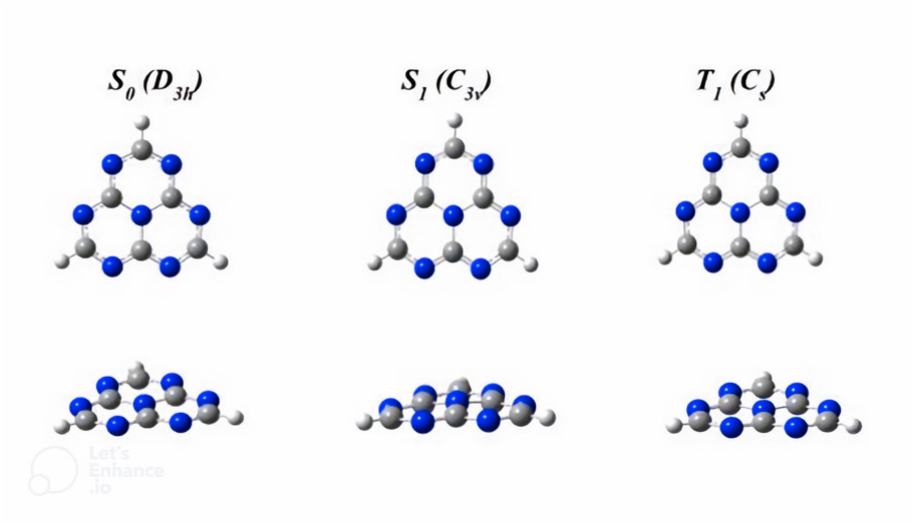

Figure 4.5: Two different views of the (VEM)-PCM/(TD)-DFT/M06-2X/def2-TZVP heptazine structures in toluene

lying closer to the plane if compared to the structures obtained at the M062X level. We then used the LR true minima as starting points for running geometry optimizations with VEM, for which second derivatives are not implemented. The transition from the linear response framework to the state-specific approach does not have a significant effect on the geometry.
We identified some key structural parameters to quantitatively compare the different geometries and support our conclusions.

Heptazine core dihedral (deg)								
	M06-2x/def2-TZVP			BLYP53/def2-TZVP				
state	*in vacuo*	LR-PCM		*in vacuo*	LR-PCM		VEM-PCM	
		TOL	ACN		TOL	ACN	TOL	ACN
S_1	-4.5	-3.7	-3.7	-3.8	-3.4	-2.2	-3.6	-3.1
T_1	-1.8	0.0	0.0	0.0	0.0	0.0	0.0	0.0

Table 4.8: Effect of XC-correlation functional excited state (TD)-DFT geometrical parameters: dihedral angle

Heptazine core C-N bond (Å)								
	M06-2x/def2-TZVP			BLYP53/def2-TZVP				
state	*in vacuo*	LR-PCM		*in vacuo*	LR-PCM		VEM-PCM	
		TOL	ACN		TOL	ACN	TOL	ACN
S_1	1.417	1.410	1.410	1.408	1.405	1.400	1.406	1.402
T_1	1.408	1.405	1.402	1.413	1.399	1.396	1.399	1.340

Table 4.9: Effect of XC-correlation functional on ground and excited state (TD)-DFT geometrical parameters: bond lenght

The preceeding discussion on heptazine cannot be extended to cyclazine. For the

latter in fact both the S_1 and T_1 true minima retain the ground state planarity and D_{3h} symmetry with each functional and excited-state PCM flavor.

4.2.4 Singlet-triplet gap

Now we proceed with the proper calculation of the energy differences between S_1 and T_1 for the IST systems of interest.
We have to provide a robust protocol to calculate the solvated first singlets and triplets, in order to account for:

- the embedding reaction to the transition density (as discussed in paragraph 3.3.1, this counts as part of a dispersion interaction);
- the embedding reaction to the excited state density difference, namely a state specific polarisation effect (see 3.3.3)
- a correction to hybrid TD-DFT energy to account for dynamic correlation.

The final definition of excited state adiabatic energy arises from the considerations above as:

$$E(ExS)_{SSpol+disp} = E(SCF)_{MP2} + \omega^{SS}_{VEM} + \Delta\omega_{LR} + \Delta\omega_{MP2} \tag{4.1}$$

The values calculated using equation 4.1 are now reported in tables 4.10 and 4.11.

	heptazine					
in vacuo	LR-PCM		ss-pol+disp		XMS-CASPT2	
	TOL	ACN	TOL	ACN	TOL	ACN
-23	44	-18	-5	139	-188	-181

Table 4.10: Adiabatic ΔE_{ST} (in meV) computed with TD-DFT/B2PLYP/def2-TZVP, on TD-DFT/BLYP53/def2-TZVP geometries and multiconfigurational benchmarks

	cyclazine			
in vacuo	LR-PCM		ss-pol+disp	
	TOL	ACN	TOL	ACN
86	0	5	72	66

Table 4.11: Adiabatic ΔE_{ST} (in meV) computed with TD-DFT/B2PLYP/def2-TZVP, on TD-DFT/BLYP53/def2-TZVP geometries

In accordance with what had already been found by Pollice et al.[8] cyclazine fails to exhibit singlet-triplet inversion at the TD-DFT level, even when treated in the double-hybrid B2PLYP framework. Therefore, any conclusion we can draw about the solvent effect in the case of cyclazine is strongly biased by the inadequacy of the electronic structure method.
Heptazine, on the other hand, presents a negative ΔE_{ST} at this level of theory both *in vacuo* and with PCM solvation. Our considerations will not be focused on the electronic structure method, which proves sufficient for the modelling of this IST substrate, but will revert on the solvent description. If we analyse the data presented in table 4.10 we can see that a standard LR-PCM calculation does not produce a ST inversion for toluene solvation ($\epsilon = 2.38$ at 298 K). On the other hand, the **ss-pol+disp** protocol is qualitatively consistent with CASPT2 calculations and produces a negative ΔE_{ST}. On the other hand, in the case of a high polarity solvent such as acetonitrile ($\epsilon = 37.5$ at 298 K), the **ss-pol+disp** description reverts the sign of ΔE_{ST} in contrast to LR-PCM. Despite what might seem at first glance, this actually represents a strength of the **ss-pol+disp** protocol. In fact, at higher computational levels, we can see that the transition from a less polar to a more polar environment disfavors the singlet-triplet inversion. This trend is accurately reproduced by our method but not by the linear response approach.
Moreover, since various studies have reported that the effect of molecular symmetry on ST inversion is negligible and that adiabatic corrections to excited state energies have a limited impact on the magnitude of the ST gap, we also calculated *vertical* ΔE_{ST} with the **ss-pol+disp** approach. We simply applied equation 4.1 using vertical rather than adiabatic ω_{VEM}^{SS} values.

molecule	*in vacuo*	LR-PCM		ss-pol+disp	
		TOL	ACN	TOL	ACN
heptazine	-11	-19	-15	-18	-15

Table 4.12: Vertical ΔE_{ST} (in meV) computed with TD-DFT/B2PLYP/def2-TZVP, on DFT/M06-2X/def2-TZVP geometries

We can now make some considerations comparing adiabatic values with vertical estimates from table 4.12. What we observe for heptazine in gas phase is consistent with the findings previously reported by Jacquemin[11]. Considering adiabatic effects does not alter the sign of the singlet-triplet gap, but it increases its absolute value. However, when solvent relaxation effects are introduced, the picture changes. Indeed, it becomes evident that when the solvent is equilibrated with the excited state and a state-specific correction is introduced, the triplet energies are excessively

stabilized with respect to the singlet energies. This effect goes in the opposite direction to the prediction of the ST inversion. In the case of a highly polar environment, this discrepancy might be so pronounced that the inclusion of the MP2 correction for dynamic correlation is insufficient to reverse the sign of the ΔE_{ST}.

Chapter 5

Application on systems of experimental interest

Since the **ss-pol+disp** protocol has been successfully benchmarked on model molecules, we proceed with the application to a number of fluorescent substituted triangulenes. For each of the substrates presented in this part of the study pioneering experimental evidence of a negative ΔE_{ST} has been found. Measuring the singlet-triplet inversion is a non-trivial task[5–7] and this explains the limited amount of experimental literature as well as the importance of having efficient computational screening methods. The following section contains the computational results for experimentally promising IST systems, each individually presented and discussed. In addition to the computation of the singlet-triplet gap, radiative and non-radiative rates were also calculated for substrates that exhibited a negative ΔE_{ST} to gather a more comprehensive picture of the molecular properties of IST systems and compare computational results with additional experimental evidences.

5.1 Computational details

For the calculation of adiabatic singlet-triplet gaps we proceeded in close analogy to section 4 and performed all calculations with Gaussian16.[49]
Ground state geometries were optimised at B3LYP/cc-pvtz in gas phase and using PCM for toluene and acetonitrile solvation. Then, S_1 and T_1 states were optimised at M06-2X/def2-TZVP.
Single point excited state energies were then calculated using BLYP53/def2-SVPP and both with LR and VEM PCM. B2PLYP/def2-SVPP energies were also calculated to apply equation 4.1. The choice to perform these calculations using a double-zeta basis set will be further substantiated in the following paragraph and was made out of necessity: the computational resources at hand proved not suffi-

cient in terms of memory storage requirements and forced us to reduce the number of basis functions used to describe the system.
Fluorescence rates were calculated with ORCA 6.0 at M06-2X/def2-SVP, resorting to the Resolution of Identity approximation (RI). Only the LR scheme is implemented in the software used and therefore no comparisons between solvation methods could be made.
For the calculation of non-radiative rates we used the code FCClasses3[62]. We re-optimised S_0 at DFT/M06-2X/Def2-TZVP and extracted S_1 and T_1 gradients from LR-PCM calculations. DFT/M06-2X/Def2-TZVP ground state geometries were also used to calculate vertical **ss-pol+disp** ST gaps.
Since the calculation of ISC and rISC constants requires knowledge of the Spin-Orbit Coupling (SOC) constant, we relied on CASSCF(14,12) followed by XMS-CASPT2 calculations on the heptazine core of the molecule to then estimate the SOC for the extended system. These were performed with the def2-TZVP basis set using OpenMolcas.[63]

5.2 Results and Discussion

5.2.1 HAP-3MF

The heptazine-based chromophore 2,5,8-tris(4-fluoro-3-methylphenyl)-1,3,3a,4,6,7,9-heptaazaphenalene (HAP-3MF, shown in figure 5.1) is generally regarded as the first inverted singlet-triplet emitter implemented in OLEDs.[64]This substrate experimentally exhibited a negative ΔE_{ST} in toluene (-220 meV) and in acetonitrile (-190 meV) on the basis of a meticulous investigation of its fluorescence and phosphorescence spectra.[6]

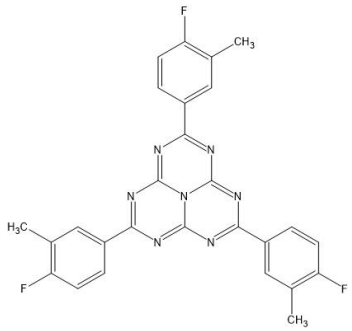

Figure 5.1: Molecular structure of 2,5,8-tris(4-fluoro-3-methylphenyl)-1,3,3a,4,6,7,9-heptaazaphenalene (HAP-3MF)

Here we present the acquired computational evidence on the substrate. First of all, it is important to underline that, in analogy to heptazine and cyclazine, the transition

to the first singlet (table 5.1) possesses very weak oscillator strength, regardless of the embedding, at each level of theory. Therefore, higher electronic states are excited and subsequently decay to S_1 through non-radiative mechanisms. S_1 is then involved in the radiative and non-radiative processes that characterise IST emitters.

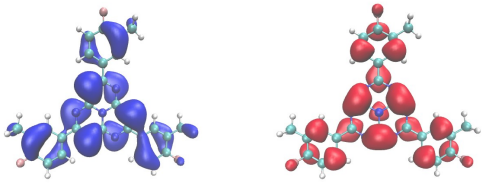

Figure 5.2: Visualisation of HOMO and LUMO of HAP-3MF with an isovalue of 0.02 a.u.

HAP-3MF	S_1			T_1		
	in vacuo	TOL	ACN	*in vacuo*	TOL	ACN
ω_0	3.166	3.195	3.235	2.991	3.020	3.058
LR	3.166	3.194	3.234	2.991	3.020	3.058
VEM	3.166	3.180	3.224	2.991	3.004	3.046

Table 5.1: HAP-3MF vertical absorption energies (in eV) at TD-DFT/M06-2X/Def2-TZVP

We proceeded with the excited state optimisations and found that S_1 and T_1 do not posses high symmetry and both belong to the C_s symmetry point group. Adiabatic ΔE_{ST} were calculated on such geometries.
However, performing double-hybrid TD-DFT single point energy calculations with a triple-zeta basis set proved to be computationally unachievable with the available resources. Therefore, for consistency reasons, we carried both BLYP53 and B2PLYP calculations with the def2-SVPP basis. To show that this change of basis does not significantly influence the description of the excited state properties, we present in table 5.3 and table 5.2 a comparison of dipole and oscillator strengths at both levels.

Dipole strenghts		
State	def2-SVPP	def2-TZVP
S_1 GAS	0.0007	0.0009
S_1 TOL	0.0012	0.0015
S_1 ACN	0.0019	0.0027
S_2 GAS	10.5204	10.6764
S_2 TOL	13.0558	13.3234
S_2 ACN	15.7073	16.2133

Table 5.2: HAP-3MF dipole strengths for the first and second singlet excited state at B2PLYP/def2-SVPP and B2PLYP/def2-TZVP (all in au)

Oscillator strenghts		
State	Def2-SVPP	Def2-TZVP
S_1 GAS	0.0001	0.0001
S_1 TOL	0.0001	0.0001
S_1 ACN	0.0002	0.0002
S_2 GAS	1.1330	1.1537
S_2 TOL	1.3747	1.4044
S_2 ACN	1.6194	1.6677

Table 5.3: HAP-3MF dipole strengths for the first and second singlet excited at B2PLYP/def2-SVPP and B2PLYP/def2-TZVP (all in au)

Now that we have established that the consistency of the protocol is retained, we can discuss the results shown in tables 5.4, 5.5 for the singlet-triplet energy gap.

HAP-3MF/in vacuo	
vertical	adiabatic
-231	-334

Table 5.4: ΔE_{ST} (in meV) computed with TD-DFT/B2PLYP/def2-SVPP, on TD-DFT/M06-2X/def2-TZVP geometries

HAP-3MF/toluene		
vertical ss-pol+disp	adiabatic ss-pol+disp	experimental
-216	-316	-220

Table 5.5: ΔE_{ST} (in meV) computed with TD-DFT/B2PLYP/def2-SVPP, on TD-DFT/M06-2X/def2-TZVP geometries

Consistent with our benchmarking, our protocol demonstrates strong reliability for the prediction of singlet -triplet inversion in non-polar environments. In the case of

HAP-3MF we are able to quantitatively reproduce the experimental values of ΔE_{ST} in toluene. We can also note that the interaction with the embedding shifts ΔE_{ST} towards more positive values. On the other hand, adding adiabatic effects into the picture produces an increase in the value of ΔE_{ST}.
We then calculated the rates of HAP-3MF radiative and non-radiative transitions in toluene to also compare our estimated quantum yield with experimental data. The calculation of these constants was made using the Adiabatic Hessian model (AH) and the results therefore pertain to the adiabatic **ss-pol** description.

rate (s^{-1})	TOL
k_F	5 x 10^6
k_{IC}	5 x 10^4
k_{ISC}	4 x 10^5
k_{rISC}	7 x 10^7

Table 5.6: HAP-3MF radiative and non-radiative transition rates computed at 300K

From the rates presented in table 5.6 we obtain a quantum yield of 8%. This in in good accordance with experimental estimates of 20%[6] as well as with other predictions of around 10% made *in vacuo* and at higher levels of theory.[65] We can conclude that, despite the vertical **ss-pol** prediction of ΔE_{ST} is in higher accordance with experimental evidence, in the adiabatic picture the properties of the molecule are overall well reproduced.

5.2.2 $HzTFEX_2$

The second system we analysed in this phase of the study is again an heptazine analogue (see figure 5.3) that was experimentally determined to possess a negative ΔE_{ST} of -11 ± 2 meV. This value was determined based on the photophysical properties of the system, measured in deaerated toluene solutions. The inversion of S_1 and T_1 was also validated by various calculations: ADC(2) and complete active space with second-order perturbation theory (CASPT2) predicted an inversion of -34 meV and -184 meV, respectively.[5]

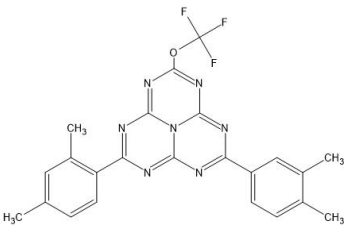

Figure 5.3: Molecular structure of $HzTFEX_2$

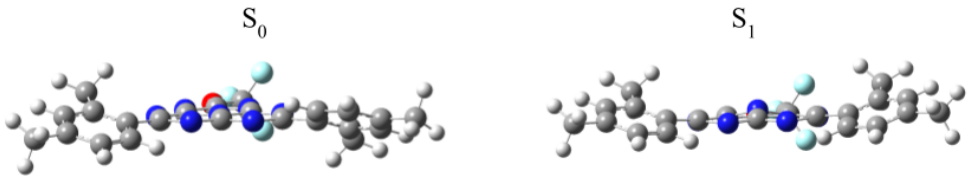

Figure 5.4: S_0 and S_1 TD-DFT/M06-2X/def2-TZVP geometries

HzTFEX$_2$/toluene		
vertical ss-pol+disp	adiabatic ss-pol+disp	experimental
15	-363	-11

Table 5.7: ΔE_{ST} (in meV) computed with TD-DFT/B2PLYP/def2-SVPP, on TD-DFT/M06-2X/def2-TZVP geometries

In the case of HzTFEX$_2$ we can see from table 5.7 how the inclusion of adiabatic effects again results not just in a higher ST gap, but reverts the sign of the ΔE_{ST} itself. The **ss-pol** estimate is around 0.3 eV larger than the experimental value, following the trend observed in other computational methods which tend to overestimate the ST gap of the molecule.
We should also note that the core of the S_1 relaxed structure of this substrate clearly possesses C_{3v} symmetry in analogy with heptazine. We can therefore assume that, in contrast with HAP-3MF, the excited state relaxation effects are more significant for this substrate.
Again, we proceeded with the calculation of radiative and non-radiative rates using **ss-pol+disp** adiabatic energies. Results are shown in table 5.8.

HzTFEX$_2$/toluene	
rate (s^{-1})	ss-pol+disp
k_F	2.3 x 10^{10}
k_{IC}	1.6 x 10^{9}
k_{ISC}	9.8 x 10^{5}
k_{rISC}	1.9 x 10^{6}

Table 5.8: HAP-3MF radiative and non-radiative transition rates computed at 300K

The estimated quantum yield of HzTFEX$_2$ in toluene is 94%. The experimental

yield of 74% is therefore slightly overestimated. This is consistent with the apparent over-stabilization of the singlet state due to adiabatic effects.

5.2.3 Pentaazaphenalene

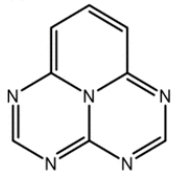

Figure 5.5: Molecular structure of 1,3,4,6,9b-pentaazaphenalene(5AP)

A direct spectroscopic quantification of the inverted singlet-triplet gap in 1,3,4,6,9b-pentaazaphenalene was recently made and yielded a result of -0.047 eV.[7]As for the other systems, several theoretical predictions of negative ΔE_{ST} were also made at different levels of theory.[7, 8, 11]
What emerged from previous computational screenings of the substrate is that computed vertical ΔE_{ST}s exhibit sharp differences from adiabatic value. For instance, Tuckova et al.[66] reported that both at the ADC(2) and CC2 level adding adiabatic correction results in slightly less negative gaps. Moreover, Wilson et al.[7] found that the application of adiabatic and ZPE corrections to EOM-CCSD transitions leads to slightly positive ΔE_{ST}s.
To the best of our knowledge, none of the values available in literature was obtained considering the interaction with the environment.

pentaazaphenalene/in vacuo		
vertical	adiabatic	experimental
50	45	-47

Table 5.9: ΔE_{ST} (in meV) computed with TD-DFT/B2PLYP/def2-TZVP, on TD-DFT/M06-2X/def2-SVPP geometries

pentaazaphenalene/toluene		
vertical ss-pol+disp	adiabatic ss-pol+disp	experimental
258	115	-

Table 5.10: ΔE_{ST} (in meV) computed with TD-DFT/B2PLYP/def2-TZVP, on TD-DFT/M06-2X/def2-SVPP geometries

We can see from the results in table 5.9 that our method is apparently not effective for the prediction of ST inversion in pentaazaphenalene. Then, the interaction with the solvent results in an increase of the value of ΔE_{ST}.
It is interesting to notice how the two systems for which the **ss-pol+disp** protocol is not effective possess a number of nitrogen atoms in the triangulene core that is inferior to 7. We can presume a form of correlation between this structural characteristic and the prediction of the inversion in the TD-DFT framework with the use of double-hybrid functionals.

Chapter 6

Conclusions and future perspectives

The research presented in this thesis aimed to investigate the still poorly understood effects of solvation on the properties of IST systems. A second consequential objective was to outline an effective and robust computational protocol in the TD-DFT framework for predicting negative gaps between singlet and triplet states in the presence of the environment, that could be applied not only to smaller model systems but also to the molecules of experimental interest. The relevance of these structures due to their perspective application in OLEDs was illustrated in Chapter 2.

The benchmarking of our method presented in Chapter 4 led us to valuable conclusions regarding both the electronic structure method and the description of the solvent's response to the solute excitation. In fact, although the use of double-hybrid functionals allows for recovering part of the dynamic correlation contribution necessary for the description of systems that violate Hund's rule, it is evident that the TD-DFT is sometimes problematic from a quantitative perspective, in contrast to the more accurate computational methods widely used in literature, such as multi-configurational techniques.

Concerning the solvent effect description, we first highlighted the significant limitation of the LR-PCM model for studying triplet excited states. On the other hand, it emerged that the state-specific model may exhibit weaknesses when describing highly polar solvents in equilibrium with the solute excited state.

In Chapter 5, we applied our protocol to the description of more extended systems for which the negative ΔE_{ST} has been experimentally observed. At this stage, we also validated our description by calculating the radiative and non-radiative transition rates.

What emerged clearly is that the choice to work within the TD-DFT framework

and to adopt the VEM as a state-specific solvation model, despite the countless advantages illustrated throughout the thesisfrom Chapter 3 has led us to encounter a series of computational bottlenecks. Overcoming these bottlenecks has had an impact on the results, if not qualitative, at least quantitative.

From a more practical point of view, it is interesting to point out that only heptazine and heptazine analogous exhibited ST inversion when treated with our model. When changing the core structure of the system by simply reducing the number of nitrogen, as in the case of cyclazine and pentaazaphenalene, the protocol proves no longer effective.

The work we have presented up to this point is part of an ongoing research project that will be included in a paper, currently under development. Among the aspects that still need to be clarified, it is crucial to find an effective way to describe the state-specific component of dispersion interactions. Moreover, to obtain increasingly accurate estimates of the ISC and rISC constants, it will be necessary to consider the vibronic spin-orbit coupling mechanism typical of heteroaromatic systems. Finally, it is worth noting that in the calculation of adiabatic energies, we considered two distinct geometries for the singlet and triplet states. Similarly, the structure used for vertical calculations corresponds to the minimum energy geometry of the ground state. Therefore, we did not explore the presence of Conical Intersections or their corresponding geometries. This aspect also represents a potential further development of the study.

Appendix A

Effects of basis set and functional

We present here the complete data from a preliminary screening on heptazine aimed at quantifying the effect of the functional and basis set on transition energies and the associated oscillator strenghts. We considered Dunning's cc-pVDZ, cc-pVTZ, aug-cc-pVDZ, and aug-cc-pVTZ.[51] The functionals analysed were B3LYP[50], M06-2X[52] and PBE0-1/3[67].
We concluded that the M06-2X double hybrid functional shows the best performances in the description of electronic excitations. Triple-zeta basis sets represent the best compromise between accuracy and computational cost. Finally, it can be noted that the Def2-TZVP[53] basis set used in other phases of the study shows performance comparable to cc-pvtz.

	cc-pVDZ	cc-pVTZ	cc-pVQZ
Number of functions	197 basis functions 450 primitive gaussians 210 cartesian basis functions	432 basis functions 727 primitive gaussians 500 cartesian basis functions	805 basis functions 1268 primitive gaussians 1015 cartesian basis functions
	AUG-cc-pVDZ	AUG-cc-pVTZ	AUG-cc-pVQZ
Number of functions	326 basis functions 592 primitive gaussians 52 cartesian basis functions	667 basis functions 1017 primitive gaussians 790 cartesian basis functions	1178 basis functions 1783 primitive gaussians 1530 cartesian basis functions

Table A.1: Number and type of functions used to describe heptazine by each of the Dunning's basis sets

TD-DFT/B3LYP Excitation energies						
Transition	cc-pVDZ	cc-pVTZ	cc-pVQZ	AUG-cc-pVDZ	AUG-cc-pVTZ	AUG-cc-pVQZ
1	2.8411	2.9013	2.9081	2.8871	2.9100	2.9099
2	3.6276	3.6804	3.6909	3.6856	3.6937	3.6929
3	3.6681	3.7409	3.7550	3.7496	3.7591	3.7584
4	3.6696	3.7424	3.7565	3.7511	3.7606	3.7599
5	4.7075	4.5975	4.5703	4.5264	4.5402	4.5395
6	4.7138	4.5980	4.5708	4.5270	4.5408	4.5400
7	4.7149	4.7109	4.7039	4.6865	4.6909	4.6895

Table A.2: Effect of basis set on TD-DFT/B3LYP excitation energies of heptazine *in vacuo* (all in eV)

TD-DFT/B3LYP Oscillator strenghts						
Transition	cc-pVDZ	cc-pVTZ	cc-pVQZ	AUG-cc-pVDZ	AUG-cc-pVTZ	AUG-cc-pVQZ
1	0.0000	0.0000	0.0000	0.0000	0.0000	0.0000
2	0.0000	0.0000	0.0000	0.0000	0.0000	0.0000
3	0.0000	0.0000	0.0000	0.0000	0.0000	0.0000
4	0.0000	0.0000	0.0000	0.0000	0.0000	0.0000
5	0.0028	0.1375	0.1403	0.1442	0.1435	0.1434
6	0.0000	0.1371	0.1400	0.1439	0.1432	0.1431
7	0.0000	0.0000	0.0000	0.0000	0.0000	0.0000

Table A.3: Effect of basis set on TD-DFT/B3LYP oscillator strenghts of heptazine *in vacuo*

TD-DFT/M06-2X Excitation energies						
Transition	cc-pVDZ	cc-pVTZ	cc-pVQZ	AUG-cc-pVDZ	AUG-cc-pVTZ	AUG-cc-pVQZ
1	3.0362	3.1461	3.1396	3.0804	3.1564	3.1419
2	4.2022	4.2705	4.2735	4.2557	4.2804	4.2748
3	4.2043	4.2727	4.2756	4.2578	4.8226	4.2769
4	4.2627	4.3153	4.3190	4.2967	4.3225	4.3188
5	5.0277	4.9876	4.9421	4.8736	4.9203	4.9075
6	5.0288	4.9886	4.9432	4.8747	4.9214	4.9086
7	5.1598	5.1771	5.1660	5.1419	5.1583	5.1534

Table A.4: Effect of basis set on TD-DFT/M06-2X excitation energies of heptazine *in vacuo* (all in eV)

TD-DFT/M06-2X Oscillator strenghts						
Transition	cc-pVDZ	cc-pVTZ	cc-pVQZ	AUG-cc-pVDZ	AUG-cc-pVTZ	AUG-cc-pVQZ
1	0.0000	0.0000	0.0000	0.0000	0.0000	0.0000
2	0.0000	0.0000	0.0000	0.0000	0.0000	0.0000
3	0.0000	0.0000	0.0000	0.0000	0.0000	0.0000
4	0.0000	0.0000	0.0000	0.0000	0.0000	0.0000
5	0.2362	0.2345	0.2373	0.2353	0.2366	0.2382
6	0.2360	0.2343	0.2373	0.2351	0.2365	0.2380
7	0.0033	0.0029	0.0032	0.0038	0.0038	0.0039

Table A.5: Effect of basis set on TD-DFT/M06-2X oscillator strenghts of heptazine *in vacuo*

TD-DFT/PBE0 Excitation energies						
Transition	cc-pVDZ	cc-pVTZ	cc-pVQZ	AUG-cc-pVDZ	AUG-cc-pVTZ	AUG-cc-pVQZ
1	3.0665	3.1223	3.1299	3.1111	3.1308	3.1312
2	4.0873	4.1401	4.1512	4.1546	4.1522	4.1516
3	4.0891	4.1417	4.1513	4.1564	4.1535	4.1528
4	4.1024	4.1432	4.1533	4.1584	4.1555	4.1548
5	4.9472	4.8862	4.8586	4.8170	4.8283	4.8277
6	4.9479	4.8870	4.8593	4.8178	4.8291	4.8285
7	5.0944	5.0951	5.0898	5.0834	5.0786	5.0768

Table A.6: Effect of basis set on TD-DFT/PBE0-1/3 excitation energies of heptazine *in vacuo* (all in eV)

TD-DFT/B3LYP Oscillator strenghts						
Transition	cc-pVDZ	cc-pVTZ	cc-pVQZ	AUG-cc-pVDZ	AUG-cc-pVTZ	AUG-cc-pVQZ
1	0.0000	0.0000	0.0000	0.0000	0.0000	0.0000
2	0.0000	0.0000	0.0000	0.0000	0.0000	0.0000
3	0.0000	0.0000	0.0000	0.0000	0.0000	0.0000
4	0.0000	0.0000	0.0000	0.0000	0.0000	0.0000
5	0.1815	0.1829	0.1851	0.1883	0.1875	0.1874
6	0.1817	0.1831	0.1848	0.1873	0.1872	0.1870
7	0.0031	0.0028	0.0031	0.0039	0.0038	0.0038

Table A.7: Effect of basis set on TD-DFT/PBE0-1/3 oscillator strenghst of heptazine *in vacuo*

Bibliography

1. Olivier, Y.; Yurash, B.; Muccioli, L.; D'Avino, G.; Mikhnenko, O.; Sancho-García, J. C.; Adachi, C.; Nguyen, T.-Q.; Beljonne, D. *Phys. Rev. Mater.* **2017**, *1*, 075602.
2. Kim, D. *International Journal of Quantum Chemistry* **2016**, *116*, 651–655.
3. De Silva, P. *J. Phys. Chem. Lett.* **2019**, *10*, 5674–5679.
4. Ehrmaier, J.; Rabe, E. J.; Pristash, S. R.; Corp, K. L.; Schlenker, C. W.; Sobolewski, A. L.; Domcke, W. *The Journal of Physical Chemistry A* **2019**, *123*, 8099–8108.
5. Aizawa, N.; Pu, Y.-J.; Harabuchi, Y.; Nihonyanagi, A.; Ibuka, R.; Inuzuka, H.; Dhara, B.; Koyama, Y.; Nakayama, K.-i.; Maeda, S.; Araoka, F.; Miyajima, D. *Nature* **2022**, *609*, 502–506.
6. Li, J.; Li, Z.; Liu, H.; Gong, H.; Zhang, J.; Li, X.; Wang, Y.; Guo, Q. *Dyes and Pigments* **2022**, *203*, 110366.
7. Wilson, K. D.; Styers, W. H.; Wood, S. A.; Woods, R. C.; McMahon, R. J.; Liu, Z.; Yang, Y.; Garand, E. *J. Am. Chem. Soc.* **2024**, DOI: `10.1021/jacs.4c05043`.
8. Pollice, R.; Friederich, P.; Lavigne, C.; Gomes, G. D. P.; Aspuru-Guzik, A. *Matter* **2021**, *4*, 1654–1682.
9. Ricci, G.; San-Fabián, E.; Olivier, Y.; Sancho-García, J. C. *ChemPhysChem* **2021**, *22*, 553–560.
10. Sanz-Rodrigo, J.; Ricci, G.; Olivier, Y.; Sancho-García, J. C. *The Journal of Physical Chemistry A* **2021**, *125*, PMID: 33401898, 513–522.
11. Loos, P.-F.; Lipparini, F.; Jacquemin, D. *J. Phys. Chem. Lett.* **2023**, *14*, 11069–11075.
12. Bedogni, M.; Giavazzi, D.; Di Maiolo, F.; Painelli, A. *Journal of Chemical Theory and Computation* **2024**, *20*, 902–913.
13. Guido, C. A.; Caprasecca, S. *International Journal of Quantum Chemistry* **2019**, *119*, e25711.
14. Guido, C. A.; Jacquemin, D.; Adamo, C.; Mennucci, B. *Journal of Chemical Theory and Computation* **2015**, *11*, 5782–5790.
15. Guido, C. A.; Rosa, M.; Cammi, R.; Corni, S. *The Journal of Chemical Physics* **2020**, *152*, 174114.
16. Cammi, R.; Corni, S.; Mennucci, B.; Tomasi, J. *The Journal of Chemical Physics* **2005**, *122*, 104513.

17. Corni, S.; Cammi, R.; Mennucci, B.; Tomasi, J. *The Journal of Chemical Physics* **2005**, *123*, 134512.

18. Marenich, A. V.; Cramer, C. J.; Truhlar, D. G. *Journal of Chemical Theory and Computation* **2013**, *9*, 3649–3659.

19. Eng, J.; Penfold, T. J. *The Chemical Record* **2020**, *20*, 831–856.

20. Uoyama, H.; Goushi, K.; Shizu, K.; Nomura, H.; Adachi, C. *Nature*, *492*, 234–238.

21. Schubert, E. F., *Light-emitting diodes (2018)*; E. Fred Schubert: 2018.

22. Wilson, J. S.; Dhoot, A. S.; Seeley, A. J. a. B.; Khan, M. S.; Köhler, A.; Friend, R. H. *Nature* **2001**, *413*, 828–831.

23. Penfold, T. J.; Dias, F. B.; Monkman, A. P. *Chem. Commun.* **2018**, *54*, 3926–3935.

24. Elliott, P.; Goldson, S.; Canahui, C.; Maitra, N. T. *Chemical Physics* **2011**, *391*, 110–119.

25. Grimme, S.; Neese, F. *The Journal of Chemical Physics* **2007**, *127*, 154116.

26. Ottochian, A.; Morgillo, C.; Ciofini, I.; Frisch, M. J.; Scalmani, G.; Adamo, C. *Journal of Computational Chemistry* **2020**, *41*, 1242–1251.

27. Sancho-García, J. C.; Brémond, E.; Ricci, G.; Pérez-Jiménez, A. J.; Olivier, Y.; Adamo, C. *The Journal of Chemical Physics* **2022**, *156*, 034105.

28. Dreizler, R. M.; Gross, E. K. U., *Density Functional Theory*; Springer Berlin Heidelberg: Berlin, Heidelberg, 1990.

29. Runge, E.; Gross, E. K. U. *Phys. Rev. Lett.* **1984**, *52*, 997–1000.

30. Kohn, W.; Sham, L. J. *Phys. Rev.* **1965**, *140*, Publisher: American Physical Society, A1133–A1138.

31. Fiolhais, C.; Nogueira, F.; Marques, M., *A Primer in Density Functional Theory*, 2003; Vol. 620.

32. Perdew, J. P.; Wang, Y. *Phys. Rev. B* **1992**, *45*, 13244–13249.

33. Perdew, J. P.; Burke, K.; Ernzerhof, M. *Phys. Rev. Lett.* **1996**, *77*, 3865–3868.

34. Becke, A. D. *Phys. Rev. A* **1988**, *38*, 3098–3100.

35. Grimme, S. *The Journal of Chemical Physics* **2006**, *124*, 034108.

36. Szabo, A.; Ostlund, N. S., *Modern Quantum Chemistry: Introduction to Advanced Electronic Structure Theory*, First; Dover Publications, Inc.: 1996.

37. Casida, M. E. In *Recent Advances in Density Functional Methods*, 1995, pp 155–192.

38. Furche, F.; Ahlrichs, R. *The Journal of Chemical Physics* **2002**, *117*, 7433–7447.

39. Tomasi, J.; Mennucci, B.; Cammi, R. *Chem. Rev.* **2005**, *105*, 2999–3094.

40. Jackson, J. D., *Classical Electrodynamics*; John Wiley & Sons: 2021.

41. Miertuš, S.; Scrocco, E.; Tomasi, J. *Chemical Physics* **1981**, *55*, 117–129.

42. Cancès, E.; Mennucci, B.; Tomasi, J. *The Journal of Chemical Physics* **1997**, *107*, 3032–3041.

43. Barone, V.; Cossi, M. *The Journal of Physical Chemistry A* **1998**, *102*, 1995–2001.

44. Cammi, R.; Mennucci, B. *The Journal of Chemical Physics* **1999**, *110*, 9877–9886.

45. Cossi, M.; Barone, V. *The Journal of Chemical Physics* **2001**, *115*, 4708–4717.

46. Caricato, M.; Mennucci, B.; Tomasi, J.; Ingrosso, F.; Cammi, R.; Corni, S.; Scalmani, G. *The Journal of Chemical Physics* **2006**, *124*, 124520.

47. Bjorgaard, J. A.; Velizhanin, K. A.; Tretiak, S. *The Journal of Chemical Physics* **2015**, *143*, 054305.

48. Marenich, A. V.; Cramer, C. J.; Truhlar, D. G.; Guido, C. A.; Mennucci, B.; Scalmani, G.; Frisch, M. J. *Chem. Sci.* **2011**, *2*, 2143–2161.

49. Frisch, M. J. et al. Gaussian˜16 Revision C.01, Gaussian Inc. Wallingford CT, 2016.

50. Becke, A. D. *The Journal of Chemical Physics* **1993**, *98*, 5648–5652.

51. Dunning Thom H., J. *The Journal of Chemical Physics* **1989**, *90*, 1007–1023.

52. Zhao, Y.; Truhlar, D. G. *Theoretical Chemistry Accounts* **2007**, *120*, 215–241.

53. Weigend, F.; Ahlrichs, R. *Phys. Chem. Chem. Phys.* **2005**, *7*, 3297–3305.

54. Grimme, S. *J. Chem. Phys.* **2006**, *124*, 034108.

55. Martin, R. L. *The Journal of Chemical Physics* **2003**, *118*, 4775–4777.

56. Zhang, Q.; Li, J.; Shizu, K.; Huang, S.; Hirata, S.; Miyazaki, H.; Adachi, C. *Journal of the American Chemical Society* **2012**, *134*, 14706–14709.

57. Hirata, S.; Sakai, Y.; Masui, K.; Tanaka, H.; Lee, S. Y.; Nomura, H.; Nakamura, N.; Yasumatsu, M.; Nakanotani, H.; Zhang, Q.; Shizu, K.; Miyazaki, H.; Adachi, C. *Nat Mater* **2015**, *14*, 330–336.

58. Zhang, Q.; Li, J.; Shizu, K.; Huang, S.; Hirata, S.; Miyazaki, H.; Adachi, C. *J. Am. Chem. Soc.* **2012**, *134*, Publisher: American Chemical Society, 14706–14709.

59. Moral, M.; Muccioli, L.; Son, W.-J.; Olivier, Y.; Sancho-García, J. C. *J Chem Theory Comput* **2015**, *11*, 168–177.

60. Guido, C. A.; Cortona, P.; Mennucci, B.; Adamo, C. *J. Chem. Theory Comput.* **2013**, *9*, 3118–3126.

61. Jacquemin, D.; Duchemin, I.; Blondel, A.; Blase, X. *Journal of Chemical Theory and Computation* **2017**, *13*, 767–783.

62. Cerezo, J.; Santoro, F. *Journal of Computational Chemistry* **2023**, *44*, 626–643.

63. Aquilante, F.; Autschbach, J.; Bast, R.; Eriksen, J. J.; Höfener, U. F.; Lindh, R.; Lau, V. K. M.; Olsen, J.; Palukaityte, A. M. S.; Pedersen, M. P. G.; Pedersen, T. B.; Sałek, D.; Sigborg, L. V. V.; Zhang, J. *J. Chem. Theory Comput.* **2016**, *12*, 1799–1809.

64. Sobolewski, A. L.; Domcke, W. *The Journal of Physical Chemistry Letters* **2021**, *12*, 6852–6860.

65. Dinkelbach, F.; Bracker, M.; Kleinschmidt, M.; Marian, C. M. *The Journal of Physical Chemistry A* **2021**, *125*, 10044–10051.

66. Tučková, L.; Straka, M.; Valiev, R. R.; Sundholm, D. *Phys. Chem. Chem. Phys.* **2022**, *24*, 18713–18721.

67. Guido, C. A.; Brémond, E.; Adamo, C.; Cortona, P. *The Journal of Chemical Physics* **2013**, *138*, 021104.

68. Guido, C. A.; Scalmani, G.; Mennucci, B.; Jacquemin, D. *The Journal of Chemical Physics* **2017**, *146*, 204106.

69. Neese, F.; Wennmohs, F.; Becker, U.; Riplinger, C. *The Journal of Chemical Physics* **2020**, *152*, 224108.